





**UNIVERSIDAD DE INVESTIGACIÓN DE TECNOLOGÍA EXPERIMENTAL  
YACHAY**

**Escuela de Ciencias Físicas y Nanotecnología**

**TITLE: Theory and Spectroscopy of Nitrogen-Doped Vertically-Aligned Multi-Walled  
Carbon Nanotubes**

Trabajo de integración curricular presentado como requisito para la obtención  
del título de Ingeniero en nanotecnología

**Autor:**

Cortez Gómez Sebastián Ismael

**Tutor:**

PhD. Chacón Julio

**Co-tutor:**

PhD. Mowbray Duncan

Urququí, agosto de 2019

Urcuquí, 28 de agosto de 2019

**SECRETARÍA GENERAL**  
(Vicerrectorado Académico/Cancillería)  
**ESCUELA DE CIENCIAS FÍSICAS Y NANOTECNOLOGÍA**  
**CARRERA DE NANOTECNOLOGÍA**  
**ACTA DE DEFENSA No. UITEY-PHY-2019-00019-AD**

En la ciudad de San Miguel de Urcuquí, Provincia de Imbabura, a los 28 días del mes de agosto de 2019, a las 10:30 horas, en el Aula Sala Capitular de la Universidad de Investigación de Tecnología Experimental Yachay y ante el Tribunal Calificador, integrado por los docentes:

**Presidente Tribunal de Defensa** Dr. PINTO ESPARZA, HENRY PAUL , Ph.D.

**Miembro No Tutor** Dr. ZAMORA LEDEZMA , CAMILO , Ph.D.

**Tutor** Dr. CHACON TORRES, JULIO CESAR , Ph.D.

Se presenta el(la) señor(ita) estudiante **CORTEZ GOMEZ, SEBASTIAN ISMAEL**, con cédula de identidad No. **2400171043**, de la **ESCUELA DE CIENCIAS FÍSICAS Y NANOTECNOLOGÍA**, de la Carrera de **NANOTECNOLOGÍA**, aprobada por el Consejo de Educación Superior (CES), mediante Resolución **RPC-SO-13-No.156-2015**, con el objeto de rendir la sustentación de su trabajo de titulación denominado: **Theory and Spectroscopy of Nitrogen-Doped Vertically-Aligned Multi-Walled Carbon Nanotubes**, previa a la obtención del título de **INGENIERO/A EN NANOTECNOLOGÍA**.

El citado trabajo de titulación, fue debidamente aprobado por el(los) docente(s):

**Tutor** Dr. CHACON TORRES, JULIO CESAR , Ph.D.

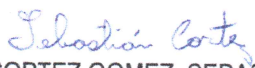
Y recibió las observaciones de los otros miembros del Tribunal Calificador, las mismas que han sido incorporadas por el(la) estudiante.

Previamente cumplidos los requisitos legales y reglamentarios, el trabajo de titulación fue sustentado por el(la) estudiante y examinado por los miembros del Tribunal Calificador. Escuchada la sustentación del trabajo de titulación, que integró la exposición de el(la) estudiante sobre el contenido de la misma y las preguntas formuladas por los miembros del Tribunal, se califica la sustentación del trabajo de titulación con las siguientes calificaciones:

Tipo	Docente	Calificación
Presidente Tribunal De Defensa	Dr. PINTO ESPARZA, HENRY PAUL , Ph.D.	9,7
Miembro Tribunal De Defensa	Dr. ZAMORA LEDEZMA , CAMILO , Ph.D.	9,3
Tutor	Dr. CHACON TORRES, JULIO CESAR , Ph.D.	8,8

Lo que da un promedio de: **9.2 (Nueve punto Dos)**, sobre 10 (diez), equivalente a: **APROBADO**

Para constancia de lo actuado, firman los miembros del Tribunal Calificador, el/la estudiante y el/la secretario ad-hoc.

  
**CORTEZ GOMEZ, SEBASTIAN ISMAEL**  
Estudiante

  
Dr. PINTO ESPARZA, HENRY PAUL , Ph.D.  
Presidente Tribunal de Defensa

  
Dr. CHACON TORRES, JULIO CESAR , Ph.D.  
Tutor

*Carlo Zamora*  
*Evelyn Tafur*

Dr. ZAMORA LEDEZMA, CAMILO, Ph.D.  
 Miembro No Tutor

CIFUENTÉS TAFUR, EVELYN CAROLINA  
 Secretario Ad-hoc

SECRETARÍA GENERAL  
 ESCUELA DE CIENCIAS FÍSICAS Y NANOTECNOLOGÍA  
 CARRERA DE NANOTECNOLOGÍA  
 UITEY-PHY-2019-00019-AD

Presidente Tribunal de Defensa  
 Miembro No Tutor  
 Tutor

Se presenta el(los) señor(ita) estudiante CORTEZ GOMEZ, SEBASTIAN ISMAEL, con cédula de identidad No. 2400171043 de la ESCUELA DE CIENCIAS FÍSICAS Y NANOTECNOLOGÍA, de la Carrera de NANOTECNOLOGÍA, aprobada por el Consejo de Educación Superior (CES), mediante Resolución RFG-SO-13-No.158-2018, con el objeto de recibir la sustentación de su trabajo de titulación denominado: Theory and Spectroscopy of Nitrogen-Doped Vertically-Aligned Multi-Walled Carbon Nanotubes, previa a la opción del título de INGENIERÍA EN NANOTECNOLOGÍA.

El citado trabajo de titulación, fue debidamente aprobado por el(los) docente(s)  
 Tutor  
 Dr. CHACON TORRES, JULIO CESAR, Ph.D.

Y recibo las observaciones de los otros miembros del Tribunal Calificador, las mismas que han sido incorporadas por el(los) estudiante y previamente cumplidos los requisitos legales y reglamentarios, el trabajo de titulación fue sustentado por el(los) estudiante y examinado por los miembros del Tribunal Calificador. Escuchada la sustentación del trabajo de titulación, que integró la exposición de el(los) estudiante sobre el contenido de la misma y las preguntas formuladas por los miembros del Tribunal, se calificó la sustentación del trabajo de titulación con las siguientes calificaciones:

Tipo	Docente	Calificación
Presidente Tribunal De Defensa	Dr. PINTO ESPARZA, HENRY PAUL, Ph.D.	9.7
Miembro Tribunal De Defensa	Dr. ZAMORA LEDEZMA, CAMILO, Ph.D.	9.3
Tutor	Dr. CHACON TORRES, JULIO CESAR, Ph.D.	8.8

Lo que da un promedio de: 9.2 (Nueve punto Dos), sobre 10 (diez), equivalente a: APROBADO

Para constancia de lo actuado, firman los miembros del Tribunal Calificador, el(los) estudiante y el(los) secretario ad-hoc

CORTEZ GOMEZ, SEBASTIAN ISMAEL  
 Estudiante

Dr. PINTO ESPARZA, HENRY PAUL, Ph.D.  
 Presidente Tribunal de Defensa

Dr. CHACON TORRES, JULIO CESAR, Ph.D.  
 Tutor

## AUTORÍA

Yo, **SEBASTIÁN ISMAEL CORTEZ GÓMEZ**, con cédula de identidad 2400171043, declaro que las ideas, juicios, valoraciones, interpretaciones, consultas bibliográficas, definiciones y conceptualizaciones expuestas en el presente trabajo; así como, los procedimientos y herramientas utilizadas en la investigación, son de absoluta responsabilidad de el/la autora (a) del trabajo de integración curricular. Así mismo, me acojo a los reglamentos internos de la Universidad de Investigación de Tecnología Experimental Yachay.

Urcuquí, agosto de 2019.



Sebastián Ismael Cortez Gómez

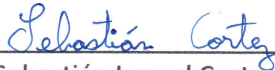
CI: 2400171043

## AUTORIZACIÓN DE PUBLICACIÓN

Yo, **SEBASTIÁN ISMAEL CORTEZ GÓMEZ**, con cédula de identidad 2400171043, cedo a la Universidad de Tecnología Experimental Yachay, los derechos de publicación de la presente obra, sin que deba haber un reconocimiento económico por este concepto. Declaro además que el texto del presente trabajo de titulación no podrá ser cedido a ninguna empresa editorial para su publicación u otros fines, sin contar previamente con la autorización escrita de la Universidad.

Asimismo, autorizo a la Universidad que realice la digitalización y publicación de este trabajo de integración curricular en el repositorio virtual, de conformidad a lo dispuesto en el Art. 144 de la Ley Orgánica de Educación Superior

Urcuquí, agosto de 2019.



Sebastián Ismael Cortez Gómez

CI: 2400171043

## **Dedication**

I want to dedicate this thesis to my family that have been my main source of love, knowledge, wisdom and good values, that made me the person I am today.

I want to dedicate this thesis also to all my friends that during my university years have always positively influenced me, and pushing me towards being a better professional.

To my supervisors, and professors that had the patience and excitement to teach me and all my colleagues their knowledge, and being a role model for professionalism, kindness, and humbleness.

Finally, I want to dedicate to all the people that in one way or another have collaborated with this project to make it happen.

## Acknowledgements

I would like to express my special appreciation to my supervisors Julio Chacón and Duncan Mowbray for all the guidance, support, and trust they had in me during the progress of this project. Duncan I want to thank specially for all the patience he had to teach me as much as he could. I want to thank my supervisor in Belgium Carla Bittencourt for pushing me to do an outstanding work in Belgium and in Italy, using her own words, I thank her for "throwing me to the lions to see if I survive", I specially thank her for teaching me the knowledge necessary to carry out part of this project. I want to thank Ayrton Sierra, Xavier Noirfalise, and Jean-François Colomer, for having contributed the synthesis of the vertically-aligned carbon nanotubes and the characterization for this thesis.

Special thanks to Paola Ayala, Juan Lobos, and Ernesto Medina that believe in me and supported me to be able to travel to the University of Mons, in Belgium, to perform the experiments necessary for this project. Thanks to the University of Mons, Materia Nova and the University of Namur for receiving me with open arms to work with them. Thanks to Kranevitter family for letting me be part of their family and care about me while I was in Belgium working in this project, without them I would have not enjoyed my stay in Belgium as much as I did. Thanks to Halé Baccouche for being not just a lab partner, but a friend, that helped me and supported me during my lab hours, and for having such a contagious enthusiasm.

Special thanks to my friends Alex Jamett, Antoni Páez and Bernardo Guerrero, for being the best housemates I would have wish for, always pushing me, helping me and suffering with the stressful hours working on our theses. Thanks to Charlotte Berrezueta, Cynthia Soto, Lorena Layana and Verónica Lobos for supporting me, helping me and cheering me up when I need it the most.

Most importantly, infinite thanks to my family, because despite being far away from me in distance, they are always with me in my heart and in my head. I thank them for always supporting me, caring for me, and cheering for me. To my parents, Oscar Cortez and Dolores Gómez, for being always there for me, for pushing me up to be a better professional and a better person, and for giving me all of their love. To my brothers and sister, Oscar, Adriana, Ivan and Manolo, for showing me their support each one on their own way.

Finally, I want to thank everyone that have contributing with their support in any possible way to achieve this project.

## Abstract

Carbon nanotubes (CNTs) are one of the most actively studied fields of research due to their outstanding mechanical, thermal, optical and electrical properties. The modification of the crystalline structure of CNTs by placing defects or foreign atoms in their hexagonal lattice is an effective method for tuning their electrical and mechanical properties. The addition of nitrogen, containing one additional electron as compared to carbon, has been shown to yield novel electrical and mechanical properties within CNTs. In recent years, there has been a great interest in vertically-aligned carbon nanotubes (v-CNTs) as both, a mean for inducing field emission and as a material for vacuum microelectronic devices. Growing carbon nanotubes over a large conducting surface is essential to obtain the uniform emission needed for vacuum nano-electronic devices. It is even more important to enhance the electronic properties of those v-CNTs by tuning their electronic properties via doping as shown in the case of N-doped CNTs. This project focuses on analyzing the grafting of nitrogen atoms via ion irradiation at the tips of vertically-aligned carbon nanotubes synthesized by catalytic chemical vapor deposition (CCVD). For the grafting we studied the dependence on acceleration voltages between 0.5 and 4.0 kV. We have performed a combined density functional theory (DFT) and x-ray photoelectron spectroscopy (XPS) study to systematically characterize the influence of N-doping on the local electronic and chemical structure of CNTs.

**Keywords:** X-ray photoelectron spectroscopy (XPS), density functional theory (DFT), defects, doping, ion implantation.

## Resumen

Los nanotubos de carbono (CNT) son uno de los campos de investigación más activamente estudiados debido a sus excelentes propiedades mecánicas, térmicas, ópticas y eléctricas. La modificación de la estructura cristalina de los CNT mediante la colocación de defectos o átomos extraños en su red hexagonal es un método efectivo para ajustar sus propiedades eléctricas y mecánicas. Se ha demostrado que la adición de nitrógeno, que contiene un electrón adicional en comparación con el carbono, produce nuevas propiedades eléctricas y mecánicas dentro de los CNT. En los últimos años, ha habido un gran interés en los nanotubos de carbono alineados verticalmente (v-CNT) como un medio para inducir emisión de campo y como un material para dispositivos microelectrónicos de vacío. El cultivo de nanotubos de carbono sobre una gran superficie conductora es esencial para obtener la emisión uniforme necesaria para los dispositivos nanoelectrónicos de vacío. Es aún más importante mejorar las propiedades electrónicas de esos v-CNT ajustando sus propiedades electrónicas mediante dopaje como se muestra en el caso de los CNT dopadas con N. Este proyecto se centra en analizar el injerto de átomos de nitrógeno mediante irradiación iónica en las puntas de los nanotubos de carbono alineados verticalmente sintetizados por deposición de vapor químico catalítico (CCVD). Para el injerto estudiamos la dependencia de los voltajes de aceleración entre 0.5 y 4.0 kV. Hemos realizado una teoría de densidad funcional combinada (DFT) y un estudio de espectroscopía de fotoelectrones de rayos X (XPS) para caracterizar sistemáticamente la influencia del N-doping en la estructura química y electrónica local de los CNT.

**Palabras claves:** Espectroscopía de fotoelectrones de rayos X (XPS), teoría funcional de densidad (DFT), defectos, dopaje, implantación de iones.



# Contents

<b>List of Figures</b>	<b>viii</b>
<b>List of Tables</b>	<b>ix</b>
<b>List of Papers</b>	<b>xi</b>
<b>1 Introduction</b>	<b>1</b>
1.1 Motivation . . . . .	2
<b>2 Theoretical Background</b>	<b>3</b>
2.1 Carbon Nanotubes . . . . .	3
2.1.1 Multiwalled Carbon Nanotubes . . . . .	4
2.1.2 Electronic properties of Multi-walled Carbon Nanotubes . . . . .	5
2.1.3 Synthesis of Carbon Nanotubes . . . . .	5
2.2 Density Functional Theory . . . . .	8
2.2.1 Hohenberg-Kohn Theorem . . . . .	10
2.2.2 The Kohn-Sham Equations . . . . .	11
2.2.3 Exchange-Correlation Functionals . . . . .	12
<b>3 Methodology</b>	<b>13</b>
3.1 Ion Irradiation Process . . . . .	13
3.2 Scanning Electron Microscope (SEM) Set Up . . . . .	14
3.2.1 Sample preparation for SEM . . . . .	14
3.3 X-Ray Photoelectron Spectroscopy Process . . . . .	15
3.3.1 Sensitivity and Specificity of XPS . . . . .	16
3.3.2 XPS Set Up . . . . .	17
3.3.3 XPS analysis . . . . .	19
3.4 Calculation Details . . . . .	20
3.4.1 XPS Simulation . . . . .	20

<b>4</b>	<b>Results &amp; Discussion</b>	<b>23</b>
4.1	XPS analysis and SEM measurements of pristine vertically-aligned carbon nanotubes . . . . .	23
4.2	XPS survey analysis and SEM measurements of vertically-aligned carbon nanotubes irradiated with Nitrogen . . . . .	25
4.2.1	Nitrogen Concentration as a function of the acceleration voltage of the Nitrogen Ions . . . . .	28
4.2.2	N 1s & O 1s core level spectra analysis . . . . .	28
4.3	DFT calculations: XPS simulated spectra . . . . .	33
<b>5</b>	<b>Conclusions &amp; Outlook</b>	<b>37</b>
<b>A</b>	<b>Nitrogen-Doped Carbon Nanotubes Structures</b>	<b>39</b>
A.1	Substitutional model . . . . .	39
A.2	Pyridinic model . . . . .	42
A.3	Pyrrolic model . . . . .	45
	<b>Bibliography</b>	<b>49</b>

# List of Figures

2.1	SWCNT Chirality Map . . . . .	3
2.2	MWCNT Schematic . . . . .	5
2.3	Arc-Discharge and Laser Ablation Schematic . . . . .	6
2.4	CVD Schematic . . . . .	7
2.5	CVD Growth Mechanism . . . . .	8
3.1	Ion irradiation Equipment and Schematic . . . . .	14
3.2	SEM equipment and Schematic . . . . .	15
3.3	XPS Schematic . . . . .	16
3.4	Photoelectron Emission Schematic . . . . .	17
3.5	XPS Equipment . . . . .	19
4.1	Pristine CNTs SEM micrographs . . . . .	24
4.2	XPS of Pristine CNTs . . . . .	25
4.3	SEM micrographs of Nitrogen-Doped CNTS . . . . .	26
4.4	Survey Spectra of Nitrogen-Doped CNTs . . . . .	27
4.5	Nitrogen Content Vs. Acceleration Voltage . . . . .	28
4.6	N 1s spectra of Nitrogen-Doped CNTs . . . . .	30
4.7	O 1s spectra of Nitrogen-Doped CNTs . . . . .	32
4.8	Schematics of SWCNT models . . . . .	33
4.9	Simulated N 1s and C 1s Spectra . . . . .	34
4.10	Simulated and Experimental N 1s Spectra . . . . .	35



# List of Tables

A.1	Coordinates in Å of a SWCNT with a substitutional or graphitic nitrogen. . . . .	42
A.2	Coordinates in Å of a SWCNT with a pyridinic nitrogen. . . . .	45
A.3	Coordinates in Å of a SWCNT with a pyrrolic nitrogen. . . . .	48



# List of Papers

- [1] Cortez, S.; Sierra, A.; Bittencourt, C.; Colomer, J.; Chacón-Torres, J.; Mowbray, D. Low-Kinetic Energy Ion Irradiation of vertically-aligned Carbon Nanotubes", *in preparation*, **2019**.



# Chapter 1

## Introduction

The push in material science towards nanoscale carbon materials has made carbon nanotubes (CNTs) one of the most prominent topics of research in materials science. CNTs have outstanding mechanical, electrical, thermal and optical properties. These characteristics make it highly desirable to incorporate them in the design of novel materials. New products with the added value of CNTs helps them to excel in their respective fields. For example, a winning Tour de France bicycle that uses a CNT composite, antifouling coatings, printed electronics, and more recently, electrostatic discharge shielding.<sup>1</sup> Furthermore, possible new applications are still being actively studied, such as super-capacitor electrodes, transparent conducting films, transistors, solar cells, and biosensors, among others.<sup>1-3</sup>

The synthesis of vertically-aligned carbon nanotubes (v-CNTs) creates a bridge between the extraordinary properties present in nanoscale CNTs to the performance of bulk materials.<sup>4</sup> v-CNTs have a variety of potential applications due to their alignment, ranging from field emission, vacuum microelectronic devices to super-hydrophobic surfaces and as a source for well-defined CNTs.<sup>5-9</sup>

Despite their highly desirable characteristics and the bulk properties that v-CNTs possess, the surface properties of CNTs may not be appropriate for certain applications. One of the main techniques for tuning the surface properties of CNTs is doping or functionalization with heteroatoms in their crystalline structure.<sup>10</sup> It is known that inplane doping with heteroatoms such as boron or nitrogen, apart from changing the crystalline structure of CNTs, will also modify the electronic properties of the material by introducing highly localized electronic features in the valence or conduction bands of the CNTs.<sup>11</sup> One of the most common heteroatoms for the doping of carbon nanotubes is nitrogen. Substitutional doping with a three-coordinated nitrogen in a  $sp^2$  hybridized network would result in N-type conductive CNTs, making it more reactive towards acceptor molecules, while a substitutional doping with a two-coordinated nitrogen in a  $sp^3$  network would result in a P- or N- type conductor depending on different factors. These include the level of doping, number of extracted carbon atoms and number of nitrogen atoms within the hexagonal network.<sup>10-13</sup> Furthermore, the methods by which this inplane N-doping can be acquired vary from *in-situ* methods such as arc-discharge or chemical vapor deposition (CVD) to *ex-situ* methods such as ion irradiation.<sup>11,14</sup> Unlike *in-situ* methods, ion irradiation preserves the morphology of pre-grown CNTs, and it is thus possible to control both the spatial distribution and dose content.<sup>14,15</sup> For these reasons we have selected ion irradiation as the method

for N-doping employed in this study.

To characterize the influence of nitrogen doping on v-CNTs we will perform a X-ray photoelectron spectroscopy (XPS) analysis. XPS is a method in which high energy photons irradiate the surface of the material. This high energy photon will eject electrons with a certain kinetic energy (KE) from the inner core levels of the atoms present on the surface of the analyzed material to a depth of  $\sim 12$  nm. The KE is measured by a detector and this information is used to obtain the core electron's binding energy (BE), which is a property specific to each element and chemical environment.<sup>16</sup> This allows us to know the nitrogen concentration, the different chemical species and whether they correspond to a  $sp^2$  or  $sp^3$  configuration in the crystal lattice.<sup>17</sup>

In order to facilitate, corroborate and expand our XPS analysis, we have used first-principles density functional theory (DFT) calculations. This theoretical method allows us to simulate and determine the specific chemical environments measured by XPS.<sup>18-20</sup>

## 1.1 Motivation

Recent advancements in N-doped CNTs have demonstrated the importance of chemically doping carbon materials. To keep track of the research done in this field, this work attempts to contribute by performing an extensive analysis of nitrogen doping by ion irradiation in v-CNTs, using a combined theoretical and experimental approach. By analysing XPS measurements using the theoretical insight provided by DFT calculations, we may obtain a better understanding of both the influence of nitrogen doping on the electronic properties of carbon nanotubes, and the reliability of DFT-based methods for describing XPS measurements.

## Chapter 2

# Theoretical Background

### 2.1 Carbon Nanotubes

Carbon nanotubes (CNTs) are a one-dimensional (1D) carbon allotrope and one of the most interesting members of

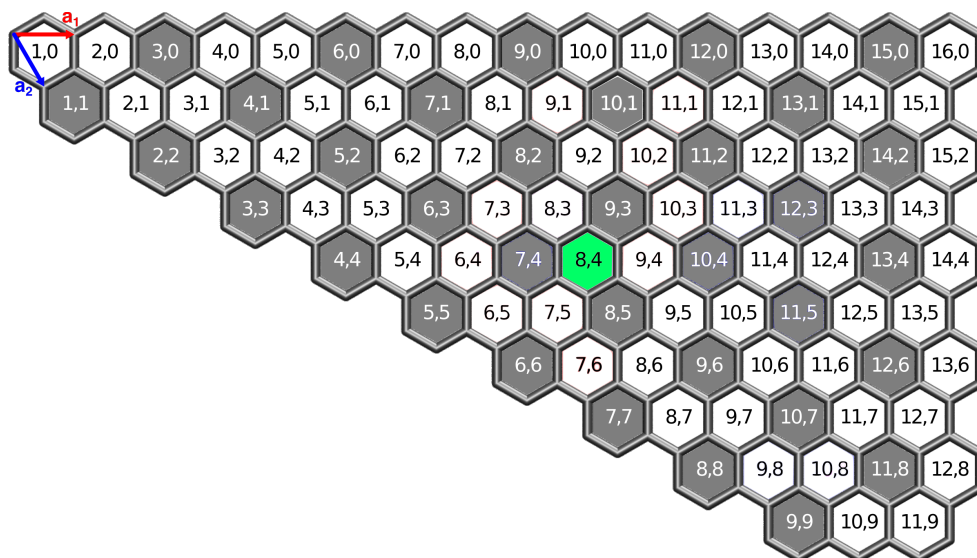


Figure 2.1: Chirality map of single-walled carbon nanotubes (SWCNTs). Metallic and semiconducting SWCNTs are marked in gray and white, respectively. The  $(8,4)$ SWCNT marked in green has been modeled throughout this work.

the nanocarbon family. CNTs exhibit a great diversity and abundance of structures and structure-property relations, even though they present a rather simple atomic and bonding structure. A single-walled carbon nanotube (SWCNT) may be thought of as a hexagonal graphene sheet rolled up into a cylindrical shape along an  $(n, m)$  lattice vector in the

graphene plane, as shown in Figure 2.1.<sup>17,21,22</sup> The pair of integers  $(n,m)$  determines both the chirality and diameter of the tube, which are key features that determine the properties of the CNT. Depending on the chirality, i.e., the angle between the lattice vector and the zigzag axis, the CNT can be semiconducting or metallic (Figure 2.1), with band gaps that can vary from  $\sim 0.5$  eV for a semiconducting CNT with a typical diameter of 1.2 nm, to  $\sim 10$  meV for a metallic CNT with a similar diameter.<sup>22-24</sup>

### 2.1.1 Multiwalled Carbon Nanotubes

Multiwalled carbon nanotubes (MWCNTs) differ from SWCNTs, in that MWCNTs are formed by multiple graphene sheets rolled up in concentric tubes. MWCNTs present electrical, thermal, optical and mechanical properties similar to their SWCNT counterparts.<sup>25,26</sup> However, MWCNTs have some important advantages for both basic science and applications. Since it is not necessary to employ magnetic catalytic nanoparticles in their synthesis, transport and magnetic measurements are more accurate for MWCNTs. The structure of multiple walls also provides MWCNTs with superior mechanical stability and greater rigidity than SWCNTs, important characteristics for scanning probe tip applications.<sup>27</sup> Moreover, for making composites with nanotubes, it is necessary first to functionalize the outer layers to create reactive sites for the formations of the composites. Even though we generate these reactive sites on the outer layers of MWCNTs, the stiffness of the internal layers will remain largely unchanged.<sup>28</sup>

Experimental studies have shown that the general structure of MWCNTs corresponds to a “Russian doll” structure consisting of concentric discrete tubes, as shown in Figure 2.2, with an average intershell spacing between 0.32 and 0.35 nm.<sup>29-31</sup> It has also been stated that CNTs larger than the stereotypical (5,5) and (9,0) can be capped, and the number of caps increases with the diameter.<sup>32,33</sup> The shells that composed the MWCNTs can be considered to be SWCNTs whether metallic or semiconducting. By statistical probability and restrictions in the diameter of the tubes, at least one of the SWCNTs is typically metallic, and therefore the whole MWCNT is usually a zero-gap metal.<sup>34</sup>

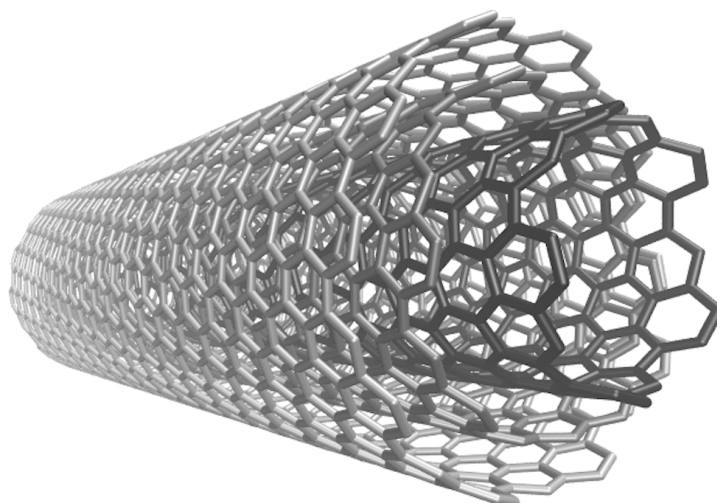


Figure 2.2: Schematic of a multi-walled carbon nanotube (MWCNT)

### 2.1.2 Electronic properties of Multi-walled Carbon Nanotubes

Since the discovery of CNTs electrical measurements of this 1D nanomaterial have proven that their electronic properties are one of the most powerful features that they possess.<sup>35,36</sup>

It is possible to configure the electrical conductivity of MWCNTs to be proportional to the electrical conductivity of individual graphene sheets. MWCNTs with diameters ( $d_t$ ) smaller than inelastic mean free path ( $l_e$ ), the electrical conductivity can be described as a ballistic transport in one dimension allowing the conductance without experiencing any scattering due to impurities or phonons, along the length of the tube. However, if  $d_t$  is higher than  $l_e$ , the predominant behavior would be a diffusive-2D conductance.<sup>37,38</sup>

Another important feature, the phase coherent length ( $l_\phi$ ), that has been determined to be approximately 250 nm (larger than the diameter of the MWCNT), by an experiment involving an important phenomena in quantum mechanics called Aharonov-Bohm effect. Nevertheless, other experiment showed the  $l_\phi$  to be approximately 20 nm by  $I$ - $V$  measurements; this inconsistency may be due to the use of poor Ohmic contacts or the quality of the MWCNTs.

Also, when doping MWCNTs, the conduction channels involved are changed as the Fermi Energy ( $E_F$ ) is shifted. There has also been noticed localization effects when doping the MWCNTs with boron, at the same time these B doped MWCNTs show a negative magneto-resistance (MR) below a temperature of approximately 60 K.<sup>39</sup>

### 2.1.3 Synthesis of Carbon Nanotubes

The preparation of high-quality carbon nanotubes have been the main goal of many research efforts. So far, arc-discharge, laser ablation and chemical vapor deposition are the principal techniques to achieve high quality carbon nanotubes.<sup>21</sup> In this section we will describe the general principles of the methods mentioned before:

- Arc Discharge and Laser Ablation:

Arc discharge and laser ablation were the first methods that allow us to synthesize CNTs in large amounts (grams). The process for arc discharge is illustrated in Figure 2.3.a) and the process of laser ablation is illustrated in Figure 3.2.b). Both techniques make us of gaseous carbon atoms generated from evaporated solid carbon. For the growth of MWCNTs it has already been demonstrated the high quality product at the gram level using the arc-discharge method. However, for the synthesis of SWCNTs it is necessary a metal catalyst. It has also been achieved the production of high-quality SWCNTs in the 1-10 grams scale using laser ablation.<sup>28,40,41</sup>

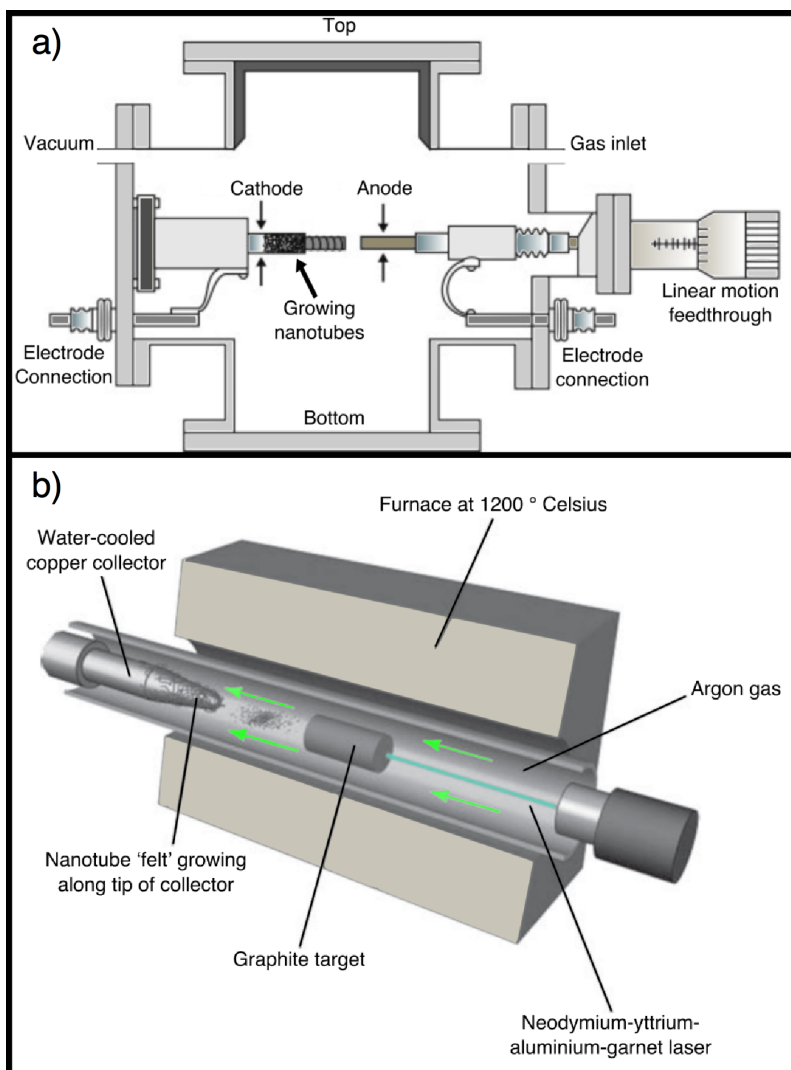


Figure 2.3: a) Schematic of arc-discharge system. b) Schematic of laser ablation system. Adapted from Ref. 21

- Chemical Vapor Deposition:

The basic principle of CVD involves the decomposition of volatile compound of carbon, using metallic nanoparticles as catalysts, that will also work as the nucleation site for the growth of the CNTs. This method being the easiest to scale up to industrial production level of SWCNTs. The synthesis of both MWCNTs and SWCNTs have been well develop using CVD. One big advantage of CVD, is that it offers more control over the structure and morphology of the CNTs. This method is illustrated in Figure 2.4.<sup>21,42,43</sup>

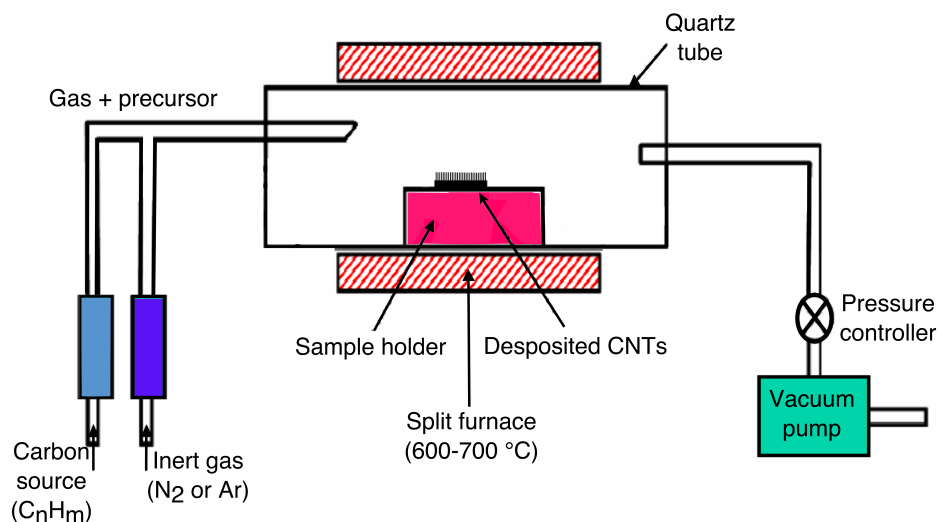


Figure 2.4: Schematic of chemical vapor deposition system. Adapted from Ref. 44

### 2.1.3.1 Synthesis of Vertically-Aligned Carbon Nanotubes by Catalytic Chemical Vapor Deposition

Vertically-aligned multi-walled carbon nanotubes were grown by thermal catalytic chemical vapour deposition technique at 750 °C in quartz tube using ethylene as carbon source, helium as carrier gas and hydrogen.<sup>45</sup> Pieces of Si wafers (1.5 cm x 1.5 cm) with native SiO<sub>2</sub> were used as the substrate for the deposition of the catalyst film that consists of 30 nm Al<sub>2</sub>O<sub>3</sub> layer as a buffer layer between the Si substrate and the Fe catalyst. A 3 nm thick Fe catalyst layer was deposited on the Al<sub>2</sub>O<sub>3</sub> layer. Both the catalyst and the buffer layer were deposited by magnetron sputtering. Fe deposition was performed using a pressure of 20 mTorr and an Ar flow of 12 sccm. The deposition of the Al<sub>2</sub>O<sub>3</sub> buffer layer was performed using a 2" in diameter alumina target, with a process pressure of 2 mTorr and an argon flow of 12 sccm.

Upon reaching the growth temperature, a flow of 500 sccm of helium was maintained in the chamber. Then, the substrate was annealed in a mixture He/H<sub>2</sub> (500/200 sccm) for 20 min at the 750 °C. This thermal annealing treatment under hydrogen allows the formation of metallic iron nanoparticles at the buffer surface, which catalyze the nucleation and growth of carbon nanotubes.<sup>46</sup> After the annealing, the mixture of ethylene/hydrogen (200/30 sccm) was introduced to synthesize the CNTs for 20 min.

The process of the formation of the nanotubes by CCVD can follow two different paths. The first one, happens when the ethylene is decomposed on the front area of the iron catalyst, producing carbon that dissolves in the catalyst (Figure 2.5.a)). The second possible outcome, comes from the strong interaction that exists between the iron catalyst and the Si substrate, the metal catalyst remains attached to the surface and the growth occurs on top of the Fe catalyst (Figure 3.2.b)).

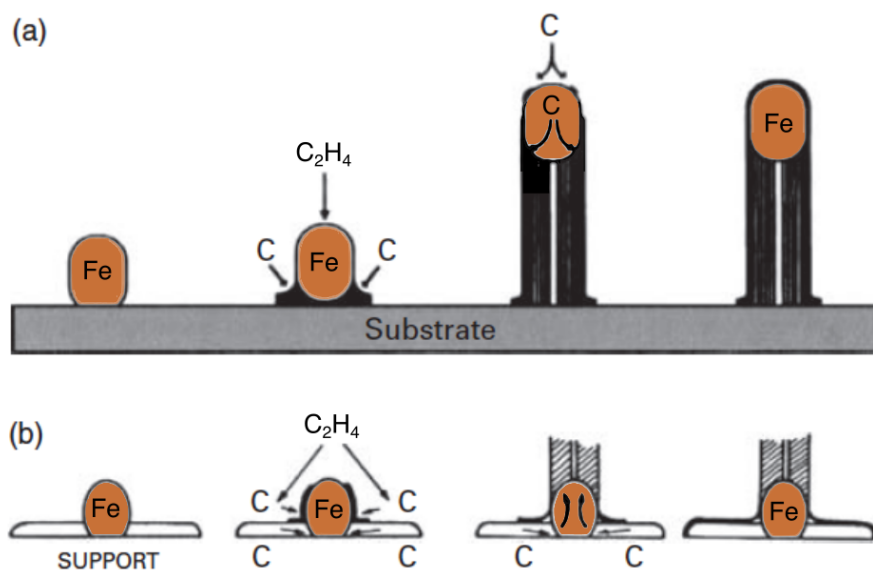


Figure 2.5: Illustration of a) the tip growth mechanism and b) the base growth mechanism of nanotube growth. Adapted from Ref. 21

## 2.2 Density Functional Theory

Density-functional theory (DFT) is one of the most popular and successful quantum mechanical approaches to modeling matter at the quantum level. For example, nowadays DFT is used to calculate the binding energy of molecules and the band structure in solids.<sup>47</sup>

To have a basic idea of how DFT works, we will be discussing some elementary concepts in quantum mechanics. We have already learned that all the information that can be obtained about a given system is contained in the system's wavefunction. Starting from the Born-Oppenheimer approximation, we can consider the contribution of the nuclei as a potential  $V_{ext}(\mathbf{r})$  acting on an electron at  $\mathbf{r}$ , since the nuclei are much heavier than the electron. In this way, the wave function for a system will only depend on the electronic coordinates.<sup>48</sup> Hence, the non-relativistic wave

function for a single electron moving in a potential  $V(\mathbf{r})$  is calculated using the Schrödinger's equation

$$\left[ -\frac{\hbar}{2m} \nabla_{\mathbf{r}}^2 + V_{ext}(\mathbf{r}) \right] \psi(\mathbf{r}) = \varepsilon \psi(\mathbf{r}). \quad (2.1)$$

For a system with more than one electron, Schrödinger's equation becomes

$$\left[ \sum_i^N \left( -\frac{\hbar}{2m} \nabla_{\mathbf{r}_i}^2 + V(\mathbf{r}_i) \right) + \sum_{i<j} U(\mathbf{r}_i, \mathbf{r}_j) \right] \Psi(\mathbf{r}_1, \mathbf{r}_2, \dots, \mathbf{r}_N) = E \Psi(\mathbf{r}_1, \mathbf{r}_2, \dots, \mathbf{r}_N) \quad (2.2)$$

where  $N$  is the number of electrons and  $U(\mathbf{r}_i, \mathbf{r}_j)$  is the electron-electron interaction. For any system interacting via the coulomb interaction we have

$$\hat{U} = \sum_{i<j} U(\mathbf{r}_i, \mathbf{r}_j) = \sum_{i<j} \frac{q^2}{|\mathbf{r}_i - \mathbf{r}_j|}. \quad (2.3)$$

In the same way we have the kinetic energy operator that will be the same for any non-relativistic system.<sup>49</sup>

$$\hat{T} = -\frac{\hbar^2}{2m} \sum_i \nabla_{\mathbf{r}_i}^2 \quad (2.4)$$

Whether we are working with an atom, a molecule, or a solid; these will depend only on the potential  $V(\mathbf{r}_i)$ . For example, for an atom our potential is

$$\hat{V} = \sum_i V(\mathbf{r}_i) = \sum_i \frac{Qq}{|\mathbf{r}_i - \mathbf{r}|}, \quad (2.5)$$

where  $Q$  is the nuclear charge and  $\mathbf{R}$  is the nuclear position.<sup>50</sup> For a molecule the potential  $V(\mathbf{r}_i)$  is written as

$$\hat{V} = \sum_i V(\mathbf{r}_i) = \sum_{ik} \frac{Q_k q}{|\mathbf{r}_i - \mathbf{R}_k|}, \quad (2.6)$$

where the sum on  $k$  extends over all nuclei in the system, each with a charge  $Q_k$  and position  $\mathbf{R}_k$ . It is only the spatial arrangement of the  $\mathbf{R}_k$  that differentiates a molecule from a solid system.<sup>51</sup> Equivalently, it is only through "U" that the quantum mechanics of the single-body problem (2.1) is different from the more complex many-body problem (2.2).

We can summarize the quantum-mechanical approach to Schrödinger's equation (SE) by the following sequence

$$V_{ext}(\mathbf{r}) \xrightarrow{SE} \psi(\mathbf{r}_1, \mathbf{r}_2, \dots, \mathbf{r}_N) \xrightarrow{\langle \psi | \dots | \psi \rangle} \text{observables}. \quad (2.7)$$

In other words, we specify our system by choosing  $V_{ext}(\mathbf{r})$ , substitute our potential into Schrödinger's equation, solve for the wave function  $\psi$ , and use the expectation values of the operators with  $\psi$  to calculate the observables.

One of the observables that we can calculate in this way is the electron density, that is the central quantity of DFT

$$n(\mathbf{r}) = N \int d^3 \mathbf{r}_2 \int d^3 \mathbf{r}_3 \dots \int d^3 \mathbf{r}_N \psi^*(\mathbf{r}, \mathbf{r}_2, \dots, \mathbf{r}_N) \quad (2.8)$$

Due to the inherent difficulty in solving the many-body problem, several methods have been developed for solving (2.2), such as, configuration interaction (CI) methods based on diagrammatic perturbation theory. The problem with these methods lies in their computational complexity, which makes their efficient application to large and complex systems unfeasible.<sup>52</sup>

This is where as a viable alternative DFT deserves to be considered. DFT recognizes that nonrelativistic Coulomb systems only differ by their external potential  $V_{ext}(\mathbf{r})$ , and provides a recipe for describing the operators  $\hat{T}$  and  $\hat{U}$ . Moreover, it gives us a way to map a many-body problem, with  $\hat{U}$ , into a single-body problem, without  $\hat{U}$ .<sup>53</sup>

$$n(\mathbf{r}) \rightarrow \psi(\mathbf{r}_1, \dots, \mathbf{r}_N) \rightarrow V_{ext}(\mathbf{r}), \quad (2.9)$$

### 2.2.1 Hohenberg-Kohn Theorem

At the heart of DFT is the Hohenberg-Kohn theorem. Hohenberg and Kohn derived the fundamentals of DFT that allow us to express the Hamiltonian as a functional of  $n(\mathbf{r})$ . This statement is based in two main theorems: (1) “there exists a one-to-one correspondence between the external potential  $V_{ext}(\mathbf{r})$  and the electron density  $n(\mathbf{r})$ ”; and (2) “the ground electron density can be found by using a variational principle”.<sup>54</sup>

From the first theorem we can write the energy  $E_V$  as a function of the electron density  $n(\mathbf{r})$  for a given external potential  $V_{ext}(\mathbf{r})$ :

$$E_V[n] = \hat{T}[n] + \hat{V}_{ne}[n] + \hat{V}_{ee} = \int n(\mathbf{r})V_{ext}(\mathbf{r})d(\mathbf{r}) + F_{HK}[n], \quad (2.10)$$

where

$$F_{HK}[n] = \hat{T}[n] + \hat{V}_{ee}[n]. \quad (2.11)$$

From Eq. 2.11 we see that  $F_{HK}[n]$  is a universal functional of  $n(\mathbf{r})$ .

The second theorem shows that we can obtain the ground state energy of the system variationally, so that the electron density minimizes the total energy to the ground state exactly:

$$E_0[n_0] \leq E_V[n]. \quad (2.12)$$

Now suppose that we have another wave function  $\psi'$  with an arbitrary variation from  $\psi$  and its electron density is  $n'(\mathbf{r})$ , then we would obtain,

$$\langle \psi' | \hat{H} | \psi' \rangle = \int n'(\mathbf{r})V_{ext}(\mathbf{r})d(\mathbf{r}) + F_{HK}[n'] = E[n'] \geq E[n] \quad (2.13)$$

If we know  $F_{HK}[n]$ , the problem of determining the ground-state energy and density in a given external potential can be easily solved. However, a major difficulty of the many-body problem is to determine this universal functional  $F_{HK}[n]$ .

## 2.2.2 The Kohn-Sham Equations

Kohn and Sham transformed density-functional theory into a practical electronic structure theory.<sup>55</sup> Their new approach involved the use of non-interacting electrons moving in an effective field.

The universal functional  $F_{HK}[n]$  is written as a sum of the kinetic energy of non-interacting electrons ( $\hat{T}_S$ ), the Hartree energy ( $E_H$ ), and all the many-body quantum effects are put together into the exchange and correlation energy ( $E_{xc}$ ). So the energy functional obtained from the first Hohenberg-Kohn theorem becomes

$$E[n] = \int n(\mathbf{r})V_{ext}(\mathbf{r})d(\mathbf{r}) + F_{HK}[n] = \int n(\mathbf{r})V_{ext}(\mathbf{r})d(\mathbf{r}) + \hat{T}_S[n(\mathbf{r})] + E_H[n(\mathbf{r})] + E_{xc}[n(\mathbf{r})] \quad (2.14)$$

The next step in this electronic structure problem is to define an effective potential,

$$V_{eff} = V_{ext}(\mathbf{r}) + \int \frac{n(\mathbf{r}')}{|\mathbf{r} - \mathbf{r}'|}d\mathbf{r}' + V_{xc}(\mathbf{r}), \quad (2.15)$$

where  $V_{xc}(\mathbf{r})$  is the exchange and correlation (xc) potential, defined as the functional derivative of the xc energy with respect to the electron density

$$V_{xc}(\mathbf{r}) = \frac{\delta E_{xc}[n(\mathbf{r})]}{\delta n(\mathbf{r})}. \quad (2.16)$$

This leads us to the principal equation of Kohn-Sham DFT, that is, the one-electron Schrödinger-like equation:

$$\left[ -\frac{1}{2}\nabla_{\mathbf{r}}^2 + V_{eff}(\mathbf{r}) \right] \psi_i(\mathbf{r}) = \varepsilon_i \psi_i(\mathbf{r}) \quad (2.17)$$

where  $\psi_i$  are the Kohn-Sham one-electron wavefunctions, the electron density is defined as

$$n(\mathbf{r}) = \sum_{i=1}^N |\psi_i|^2, \quad (2.18)$$

and the  $\varepsilon_i$  are the energies of the Kohn-Sham one-electron orbitals. Finally, by using the resulting density  $n(\mathbf{r})$ , we can obtain the total energy through

$$E = \sum_{i=1}^N \varepsilon_i - \frac{1}{2} \iint \frac{n(\mathbf{r})n(\mathbf{r}')}{|\mathbf{r} - \mathbf{r}'|} + E_{xc}[n] - \int V_{xc}(\mathbf{r})n(\mathbf{r})d(\mathbf{r}). \quad (2.19)$$

The Kohn-Sham equations are (2.15), (2.17) and (2.18). The general procedure is to start with an initial guess of the electron density, construct the effective potential  $V_{eff}$ , which depends on  $n(\mathbf{r})$  from Eq. 2.15, and hence obtain the Kohn-Sham wavefunctions  $\psi_i$ . Using these wavefunctions, we can get a new density from Eq. 2.18, and repeat the process until we achieve self-consistency. Finally, we can calculate the total energy of the system with Eq. 2.19.

It would be possible to obtain the exact ground state density and energy if we knew all the terms. Unfortunately, we do not know the exact form of the xc functional,  $E_{xc}[n(\mathbf{r})]$ . This term includes all the purely quantum mechanical aspects of the electron-electron interaction along with corrections to the kinetic energy of the many-body system. Since the exact form of  $E_{xc}$  remains unknown, it is necessary to approximate it.

### 2.2.3 Exchange-Correlation Functionals

Since the birth of DFT, many different kinds of approximations for  $E_{xc}$  have been proposed. Today there exist a plethora of approximate functionals with different levels of complexity. Luckily there is a useful way for categorizing the many and varied  $E_{xc}$  functionals that exist known as “Jacob’s ladder”.

Some of the most common types of exchange-correlation functionals in widespread use are described in the following subsections.

#### 2.2.3.1 Local Density Approximation (LDA)

In the local density approximation (LDA) the electronic xc energy is a functional of the local density  $n(\mathbf{r})$  only, and the corresponding exchange-correlation energy is obtained from the uniform electron gas, which has the same density everywhere. This approximation is only valid for systems with slowly varying densities, and overestimates cohesive energies of metals and insulators by 10%-20% and H bond energies by >50%. Long range van der Waals interactions are not captured.<sup>56-58</sup>

#### 2.2.3.2 Generalized Gradient Approximation (GGA)

In the generalized gradient approximation (GGA), the electronic xc energy is taken to be a functional of both the local density  $[n(\mathbf{r})]$  and the gradient of the density  $[\nabla n(\mathbf{r})]$ .<sup>59</sup>

GGAs describe hydrogen bonded systems and other systems that are weakly bounded much better than LDA. Usually it underestimates cohesive energies of metals and insulators. For systems with larger density gradients, the performance of functionals depends heavily on the choice of the enhancement function. Long-ranged van der Waals interactions are poorly described.<sup>60,61</sup>

#### 2.2.3.3 Meta-Generalized Gradient Approximation (meta-GGA)

The electronic xc energy is taken to be a functional of the local density  $[n(\mathbf{r})]$ , the gradient of the density  $[\nabla n(\mathbf{r})]$ , and the kinetic energy density  $[\nabla\psi n(\mathbf{r})]$ . This method has a small improvement over GGAs. It gives better surface energies and in some cases describes weakly bounded systems better than GGAs.<sup>62-64</sup>

#### 2.2.3.4 Hybrid-Generalized Gradient Approximation (hybrid-GGA)

This method is a hybrid mixture of GGA xc functionals with some fraction of Hartree-Fock exchange. It fixes self-interaction errors to some extent and provides much better band gaps and reaction barrier heights than LDA and GGAs. The description provided for metals are worse than GGAs and it is computationally expensive to apply for periodic systems.<sup>65-67</sup>

## Chapter 3

# Methodology

### 3.1 Ion Irradiation Process

The ion implantation was performed with an ion source IS 40C1 Prevac system in Materia Nova laboratory in Mons, Belgium (Figure 3.1.a)). The different parts of the Ion irradiation system are shown in Figure 3.2.b).

In this source, a nitrogen plasma was created, a total ion implantation time was set at 1 hour with an emission current of 5 mA. While different acceleration voltages were applied in the range of 0.5 KV to 4KV for the different samples of vertically-aligned carbon nanotubes. The base vacuum pressure in the preparation chamber vary from  $10^{-7}$  mbar to  $10^{-8}$  mbar. During functionalization, the pressure of  $N_2$  gas was set at  $1.2 \times 10^{-6}$  mbar.

The samples were mounted along the same direction in all cases, with the tips of the v-CNTs facing the nitrogen ion beam at a working distance around 3 cm in the normal direction.

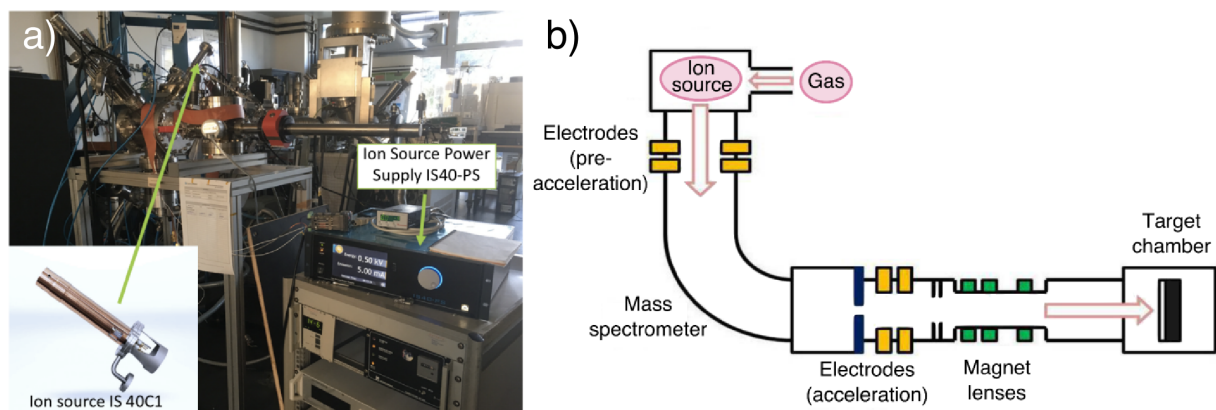


Figure 3.1: a) Ion source IS 40C1 and Ion Source Power Supply IS40-PS Prevac system at Materia Nova Laboratory. b) Schematic of ion irradiation process. Adapted from Ref. 68

## 3.2 Scanning Electron Microscope (SEM) Set Up

JEOL JSM-7500F is a simple operation Field Emission Scanning Electron Microscope (Figure 3.2.a)), that features a special optical system that can collimate the electron beam, even at a low acceleration voltage. It includes a high brightness conical Field-emission gun and low aberration conical objective lenses. The system is capable of observe the sample up to  $\times 1000000$  with a resolution of 1 nm. The different parts of a SEM are shown in Figure 3.2.b)<sup>69</sup>

The equipment also possesses an r-filter, that includes filtering electrodes, and control electrodes for secondary electrons and backscattered electrons.<sup>69</sup>

JEOL JSM-7500F is also equipped with a five motor controlled stage, that has an enhanced stability against floor vibrations.<sup>69</sup>

### 3.2.1 Sample preparation for SEM

V-CNTs did not need special preparation before for the scanning electron microscope. Samples were put directly to sample holder to be analyzed.

For the obtention of the SEM micrographs, the Standard Sb mode was selected, this mode allows to detect pure secondary electrons, that is the most convenient mode for the study of suface morphologies. We used an acceleration voltage of 15 kV.

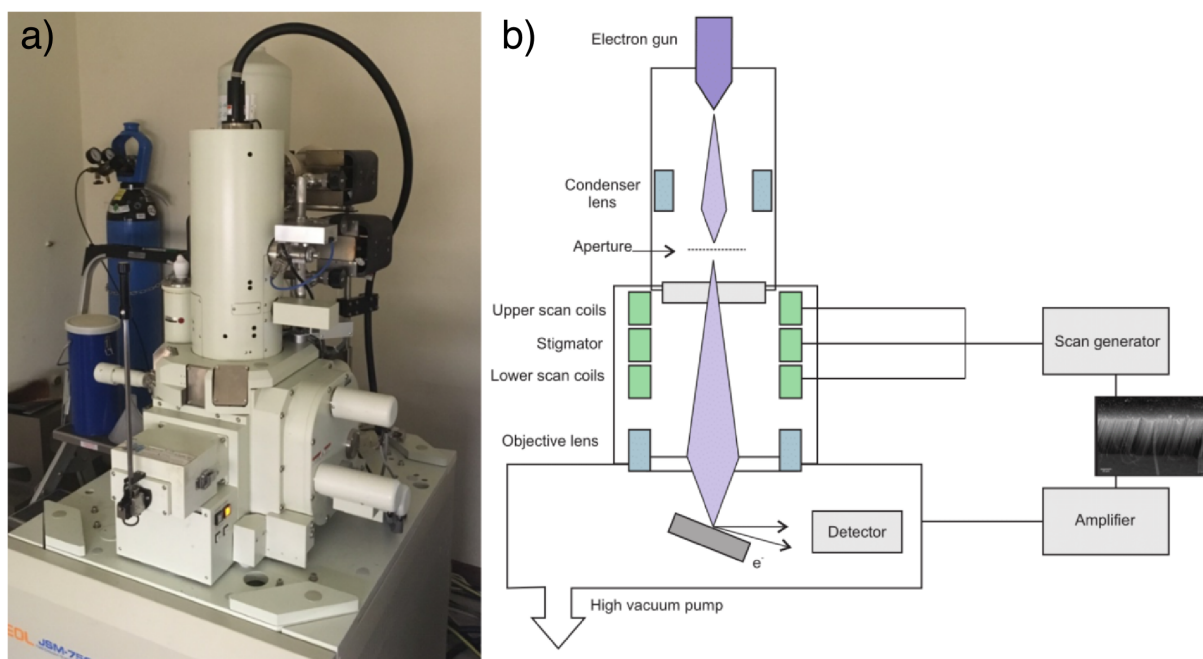


Figure 3.2: a) JEOL JSM-7500F-Field Emission Scanning Electron Microscope at University of Namur. b) Schematic of scanning electron microscopy principle. Adapted from Ref. 70

### 3.3 X-Ray Photoelectron Spectroscopy Process

X-ray Photoelectron Spectroscopy (XPS), also known as Electron Spectroscopy for chemical Analysis (ESCA), represents the most heavily used electron spectroscopic technique used to measure the elemental composition in the surface of a material (1-12 nm depth).<sup>71,72</sup>

The basic principle of XPS relies on shooting of a high energy photon that can ionize an atom, and therefore eject a free electron from the most inner shells. Depending on the energy of the photon, and the measured kinetic energy, and using Einstein's photoelectric law:<sup>71-73</sup>

$$K.E._{XPS} = h\nu - \phi_{XPS} - B.E._{XPS}, \quad (3.1)$$

where  $K.E._{XPS}$  is the kinetic energy of the detected photoelectron,  $h\nu$  represents the energy of the photon,  $B.E._{XPS}$  is the binding energy of the photoelectron, and  $\phi_{XPS}$  is the work function of the instrument, we take this quantity under the assumption that the the measured sample is conductive and it is in physical contact with the instrument Figure 3.3.<sup>71</sup>

We are able to know the Binding Energy corresponding to that electron. This binding energy is specific for the

for the element and the chemical environment. The quantitative analysis requires the measurement of relative peak intensities, this will allow us to know the concentrations of the different elements and the chemical species they belong to.<sup>71,72</sup>

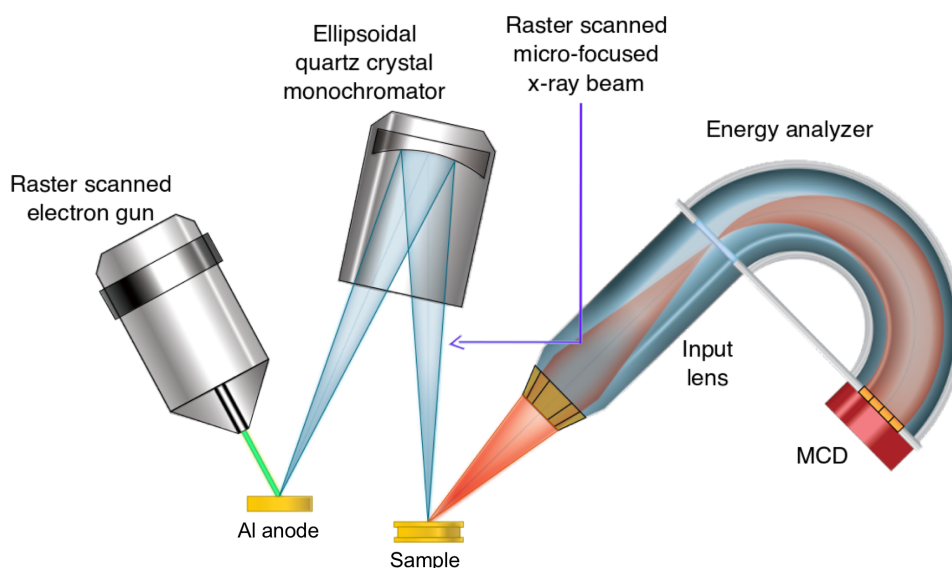


Figure 3.3: Schematic representation of the operation principle of XPS. Adapted from Ref. 74

### 3.3.1 Sensitivity and Specificity of XPS

The characteristics that allow the XPS method to determine and quantify the elemental composition and chemical speciation over the 12 nm depth of the surface of any solid, assuming that each element of interest is present with at least 0.05 atomic %, are:

- Surface specificity or the capability to separate the signal coming from the 12 nm of the surface from the signal coming from the underlying layer of the material.<sup>71</sup>
- Sensitivity or the capacity to detect the signal of interest from the analyzed material given the limitation of the small volume from which the signal proceeds.<sup>71</sup>

Surface specificity is the result of the finite path of an electron within a solid before it loses some of its kinetic energy. It should be noted that x-rays can penetrate several micrometers below the surface area of 12 nm that we mentioned before, the issue comes from some ejected photoelectrons, that if they lose some energy, their signal will disappear in the spectral background. Thus, the discrete signals or spectral lines that remain in the spectra

will correspond to the different atoms present in the surface region of the material. These concepts are shown in Figure 3.4<sup>71</sup>

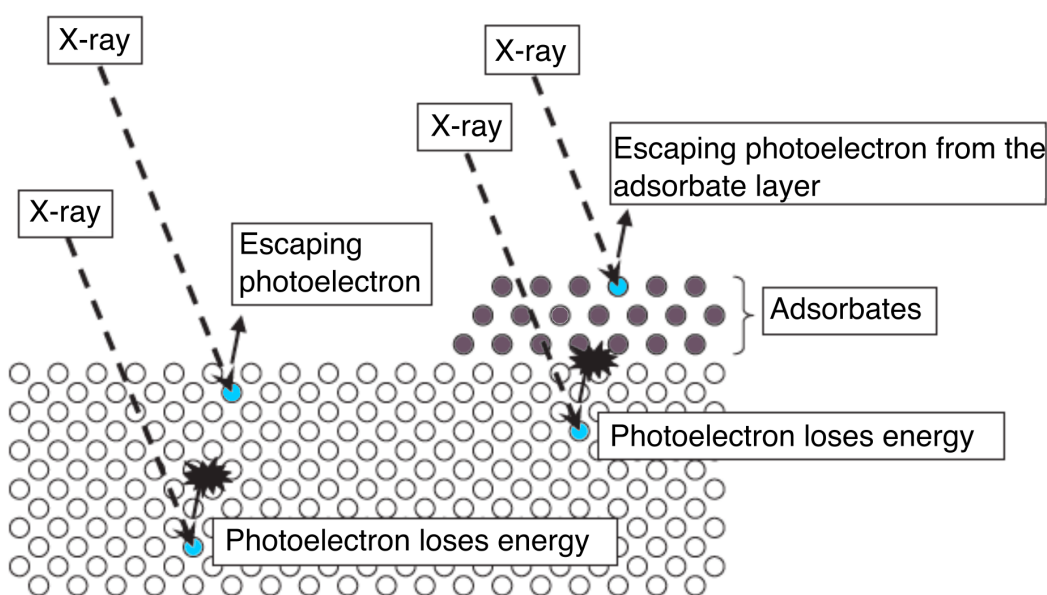


Figure 3.4: Schematic of photoelectron emission from a solid material. Adapted from Ref. 16

Sensitivity is mainly a function of the photoemission cross-section of the ejected electrons. The photoemission cross-section primarily refers to the probability to produce a photoelectron given the photon energy. Hence, elements with low photoemission cross-section such as hydrogen and helium are not detectable by XPS. The sensitivity of the XPS can also be affected by the vacuum under which the analysis chamber is at the moment of the measurement, since this controls the density of molecules in the gas phase and, therefore, the fly path of the photoelectron to the detector.<sup>71,72,75</sup>

### 3.3.2 XPS Set Up

For the XPS analysis it was used an ESCA-5000 (Physical Electronics) VersaProbe system (Figure 3.5.a)).<sup>76</sup>

This XPS system is capable of providing secondary-electron imaging. This imaging is possible by focusing a X-ray beam of  $10\ \mu\text{m}$  through the entire sample. It is capable to expose features that are not noticeable by optical observation or associated to topography.<sup>76</sup>

This micro-focused X-ray beam is able to set the area of analysis for micro-area spectroscopy, large area spectroscopy, chemical-state imaging and depth profiling.<sup>76</sup>

The analysis with the ESCA-5000 VersaProbe system starts with a secondary-electron imaging of the sample. From this image we can select one or several points to perform the analysis. The resulting XPS spectra can be used to acquire chemical-state images, composition sputter depth profile, or high-resolution energy spectra for chemical analysis.<sup>76</sup>

### 3.3.2.1 XPS equipment ESCA-5000 VersaProbe

In Figure 3.5.b) are show the different accesories of the ESCA-5000 VersaProbe:<sup>76</sup>

- Scanning X-ray source
- Sample introduction chamber
- Optional intro/prep chamber
- Argon sputter ion gun
- Electron energy analyzer
- Optical Microscope
- Five axis automated sample manipulator
- Optional hot/cold version shown
- LN2 dewar for sample cooling
- Optional sample preparation chambers
- Optional C<sub>60</sub> sputter ion gun
- Optional UV light source for UPS
- Optional dual anode X-ray source
- Optional electron gun for SAM
- Optional 20 kV Ar<sub>2500</sub><sup>+</sup> gas cluster ion gun

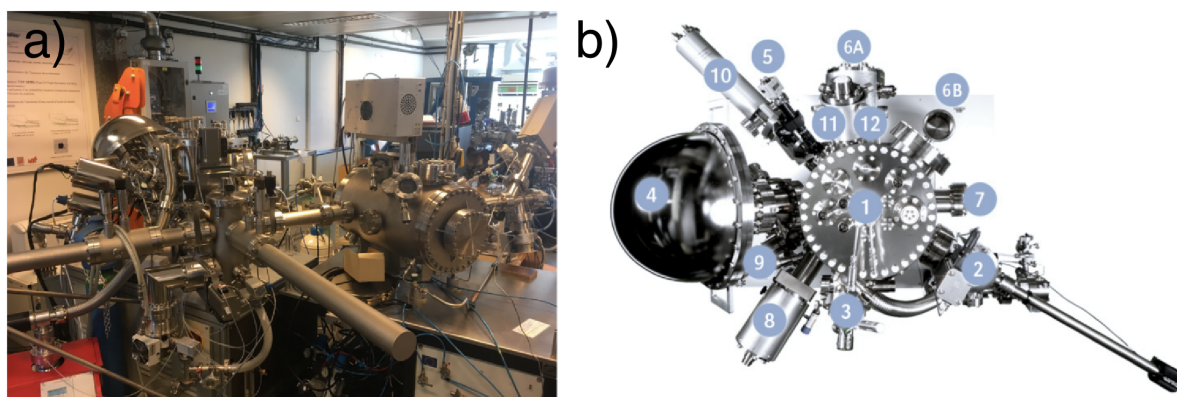


Figure 3.5: a) XPS equipment ESCA-5000 VersaProbe system at Materia Nova laboratory. b) ESCA-5000 VersaProbe components. Adapted from Ref. 77

### 3.3.3 XPS analysis

All samples of vertically aligned multiwalled-carbon nanotubes irradiated with Nitrogen ions were analyzed by XPS. The light beam used had a diameter of  $200\ \mu\text{m}$  with a power of 50 W and a voltage of 15 kV. The pressure inside the analysis chamber was  $2 \times 10^{-6}$  Pa. The XPS data were collected using a monochromatic Al K-alpha radiation at 1486.6 eV. Photoelectrons were collected at take-off angle of  $45^\circ$  (normal detection) to the surface normal.

The survey spectra was taken with a pass energy of 187.85 eV with a step of 0.5 eV, while the elements were analyzed with a pass energy of 23.5 eV (high resolution spectra) with a step of 0.2 eV. Atomic compositions were derived from peak areas using photoionization cross-sections calculated by Scofield, these were corrected for the dependence of the escape depth on the kinetic energy of the electrons and corrected for the analyzer transmission function of the spectrometer. Finally, atomic compositions were derived from peak areas after a Shirley background subtraction.

For the analysis of each element a Shirley background subtraction was implemented to obtain areas corresponding to the different chemical species. This background was chosen since it uses information from the spectrum itself. This background encompasses the general idea that as we have more electrons emitted, more electrons will be scattered. The Shirley background is well accepted, specially for this type of analysis, where the range of analysis is short and there are not doublet pairs to analyse.<sup>78,79</sup>

For peak fitting of each individual element we used a Gaussian-Lorentzian line shape, since the XPS profile is not coming entirely from the atomic level regarded, but also from the instrument and its resolution.<sup>79</sup>

### 3.4 Calculation Details

All-electron density functional theory (AE-DFT) calculations were performed using the projector augmented wave function (PAW) method implemented in the GPAW code within the GLLB-SC for the exchange and correlation (xc)-functional which is based on the PBEsol xc-functional for solids, and allows the efficient calculation of the derivative discontinuity. We employed two methods to describe the wavefunctions: Real Space and Partial Waves. All structures were relaxed until a maximum force below  $0.05 \text{ eV/\AA}$  was reached. We consider a defective semiconducting carbon nanotube as our system, the (8,4), with different types of defects: substitutional, pyridinic and pyrrolic, to simulate the x-ray photoelectron spectra.

the substitutional nitrogen (or graphitic-center nitrogen), and the pyridinic nitrogen are  $sp^2$  hybridized whereas, pyrrolic nitrogen is  $sp^3$  hybridized. The pyridinic-N is bonded to two carbon atoms in an hexagonal ring. Pyrrolic-N refers to a N atom that bonds with two carbons in a pentagonal ring. The substitutional-N refers to N atom that substitute a carbon atom in the hexagonal lattice, bonded to three carbon atoms.<sup>80</sup> These types of defects are shown in Figure 4.8

We used a  $k$ -point sampling of  $(1 \times 1 \times 9)$ , having a  $\Delta k \lesssim 0.06 \text{ \AA}^{-1}$ . This is sufficient because the modeled system is semiconducting, so the dispersion of the bands is not very significant. Moreover, what we are interested in is the all-electron core levels, which do not disperse. Thus the density of the  $k$ -point sampling is dense enough for these kind of calculations. For the relaxation of the structure we used a double- $\zeta$  polarized (DZP) basis set.<sup>81</sup> We set periodic boundary conditions along the length of the tube, and we set the electron density and Kohn-Sham wavefunctions to zero at the boundaries perpendicular to the nanotube axis. The nanotube unit cell has a length of  $18.29 \text{ \AA}$  perpendicular to the tube, and  $11.34 \text{ \AA}$  along the tube axis. The unit cell has an effective grid spacing  $h \approx 0.19 \text{ \AA}$ .<sup>82,83</sup> All possible parameter that can be set up are shown in Ref. 84

#### 3.4.1 XPS Simulation

For the calculation of the core level energies, first it is necessary to create a new set up that simulates effectively the core level electronic wavefunctions. For this, we perform an all-electron calculation on a radially symmetric real-space grid for the isolated atom. From this we obtain the all-electron radial wavefunctions, from which we generate smooth wavefunctions that are exactly the same as their all-electron counterparts outside the augmentation sphere, but orthogonal to all the other wavefunctions generated inside the augmentation sphere.

Once we have this new set up that describes accurately the core levels of the isolated atom, we have to perform a calculation for the complete system. To do this, we have two options: (1) we can perform an initial-state calculation where we model the system at the ground state where we use the Kohn-Sham eigenenergies to get the core levels and (2) a final state calculation where we model the ground state and the excited state of the system, and obtain the total energy of the core level by the difference in energy between the excited state of a particular atom and the ground state. We model this excited state by reducing the occupation of the atom's core level, i.e., creating a core-hole. To simulate this core-hole we can use one of three different methods. The simplest one is by using a full core-hole in whichever atom we are exciting. In this model, the ejected photoelectron is place into the vacuum. This method

has the advantage that the absolute binding energies are around 2% of the experimental values. However, this still amounts to a discrepancy of around 2 eV between the calculation and the experiment. This difference is enough to require a shift of the calculated binding energies when comparing to the experimental values. Another drawback of this method is that the binding energy will depend very strongly on the ability of the system to screen the core-hole. To avoid this issue, there exists the half-core hole method. This method requires to take away half an electron from the 1s level from whichever atom we are exciting. The photoelectron is assumed to be moved to the vacuum level, but in this case, it is assumed that the core-hole is partially screened within the atom. This type of calculation has the advantage of requiring less screening of the core-hole by the system. The downside is that the absolute energies will be about half of the full core-hole, meaning that only the shift between components can be compared to experiment. The last final-state method involves a full screening of the core-hole. This method differs from the full core-hole method only by moving the photoelectron to the bottom of the conduction band instead of the vacuum level. This charging of the system will result in a full screening of the core-hole, so the entire system is neutral. This suggests that the screening of the core-hole will not depend anymore on charge redistribution in the environment. This type of calculation describes better X-ray adsorption spectroscopy (XAS), meaning that this method will only describe XPS just in the case where XAS and XPS are in quantitative agreement.

For this project, we perform initial-state calculations, since this method provides all core level energies at once, while for the final-state method one would have to extract an electron in separate calculations for each atom that we wish to model. Moreover, from a computational feasibility and accuracy of results point of view, the initial-state method is preferable to describe XPS measurements.

Now, to describe this system it is necessary to implement the projector functions, which if they overlap when projected on our previous set up, we will obtain our new core level energies corresponding to the initial-state system. To do this this, we give our initial guess for the electron density, for this we can use two methods: real-space finite-difference method, that allows us to calculate directly the wave function and potential on real-space grids; and linear combination of atomic orbitals where we choose a basis set to calculate the electron density. For this project we decide to use both methods, for the second method we chose a partial waves basis set since it gives the best description for the core level, as opposed to other basis like double- $\zeta$  polarized (DZP) that gives a better description for the outer layers of the atom.<sup>85</sup>



## Chapter 4

# Results & Discussion

\* 86

In this chapter, XPS results and the SEM images are shown and discussed.

### 4.1 XPS analysis and SEM measurements of pristine vertically-aligned carbon nanotubes

The starting materials are arrays of vertically-aligned carbon nanotubes. The SEM micrographs of the vertically-aligned CNTs shown in Figure 4.1, demonstrate the vertical alignment of the sample as well as its spatial uniformity and distribution. The whole array shows rather long CNTs, each CNT in the vertically-aligned array show a mean length of  $\sim 80 \mu\text{m}$ . Furthermore, the inset of Figure 4.1 show that the MWCNTs preserve the tube morphology, in addition, the inset also shows that most of them are also very thick, presenting a mean diameter of  $\sim 30 \text{ nm}$ .

---

\*This work was performed in collaboration with Ayrton Sierra, Carla Bittencourt, Jean-François Colomer, Julio Chacón-Torres, Duncan Mowbray, and is adapted from "Low-Kinetic Energy Ion Irradiation of vertically-aligned Carbon Nanotubes", *in preparation*, **2019**.

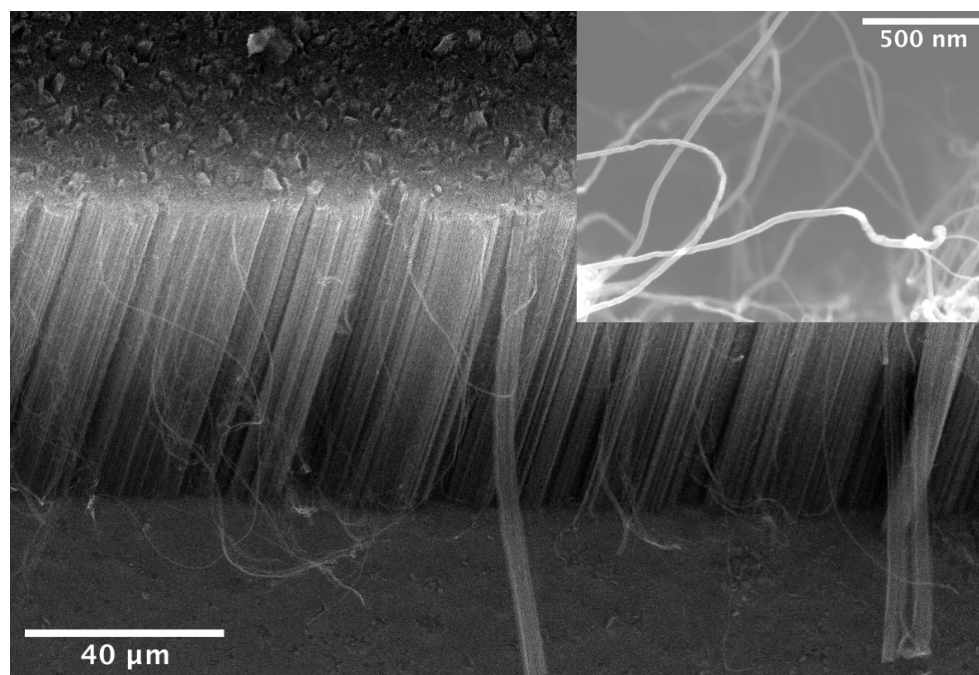


Figure 4.1: SEM of pristine vertically-aligned carbon nanotubes.

To analyze the chemical environment present in the pristine vertically-aligned CNTs, the XPS data was studied. The XPS raw data was analyzed using CasaXPS Version 2.3.17PR1.1. The XPS survey shown in Figure 4.2.a) shows two peaks. The peak at 285.23 eV corresponds to the C 1s, while the peak at 533.23 eV corresponds to the O 1s. Although, the O 1s in the survey spectra is almost not visible (Figure 4.2.a)), casaXPS detects the presence of this peak, this can be justify by the high resolution O 1s spectrum that clearly shows the presence of oxygen (Figure 4.2.b)). Showing that the pristine vertically-aligned CNTs present some oxygen contamination. To estimate the atomic percentage corresponding to the carbon and the oxygen, the areas under the peaks were calculated. A Shirley background was used to gauge the area under the peaks. The estimated atomic percentages show that 96.99% of the pristine sample is carbon, while the contamination of oxygen represents 3.01%.

The deconvolution of the O 1s and the C 1s regions is shown in Figure 4.2.b,c). The Survey, O 1s and C 1s spectra (Figure 4.2) were calibrated using the C=C  $sp^2$  (C1) of the C 1s component set at 284.18 eV by NIST XPS Database.<sup>87</sup> The C 1s consists in five components, the  $sp^2$  C=C at 284.18 eV as mentioned before,<sup>88</sup> the  $sp^3$  C-C (C2) at 284.69 eV,<sup>14</sup> two components at 285.26 eV and 288.36 eV which correspond to C-OH (C3) and O-C=O (C4) bonds respectively,<sup>88,89</sup> and at 291.07 eV the  $\pi \rightarrow \pi^*$  transition (C5), characteristic of pristine CNTs.<sup>90</sup>

The O 1s region consists in two components, the O-C=O (O1) at a binding energy of 531.64 eV, and the C-OH at a binding energy of 533.69 eV.<sup>88</sup>

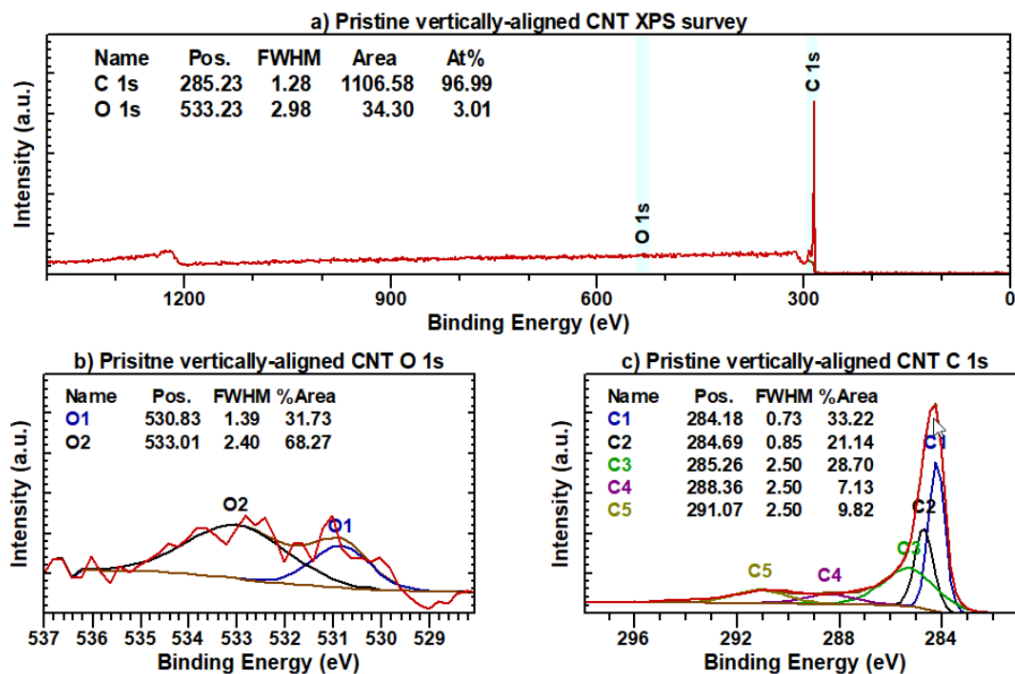


Figure 4.2: XPS a) survey, b) O 1s and c) C 1s spectra of pristine vertically-aligned CNTs.

## 4.2 XPS survey analysis and SEM measurements of vertically-aligned carbon nanotubes irradiated with Nitrogen

The SEM micrographs of the vertically-aligned CNTs after ion irradiation shown in Figure 4.3 a), b), c), and d) exhibit a bamboo-like structure, typical for nitrogen-doped CNTs, indicating that the nitrogen atoms were inserted into the carbon network. All samples show uneven compartments, that are difficult to distinguish one from the other in certain nanotubes. Other changes may be very subtle to be perceived by using SEM.<sup>91,92</sup>

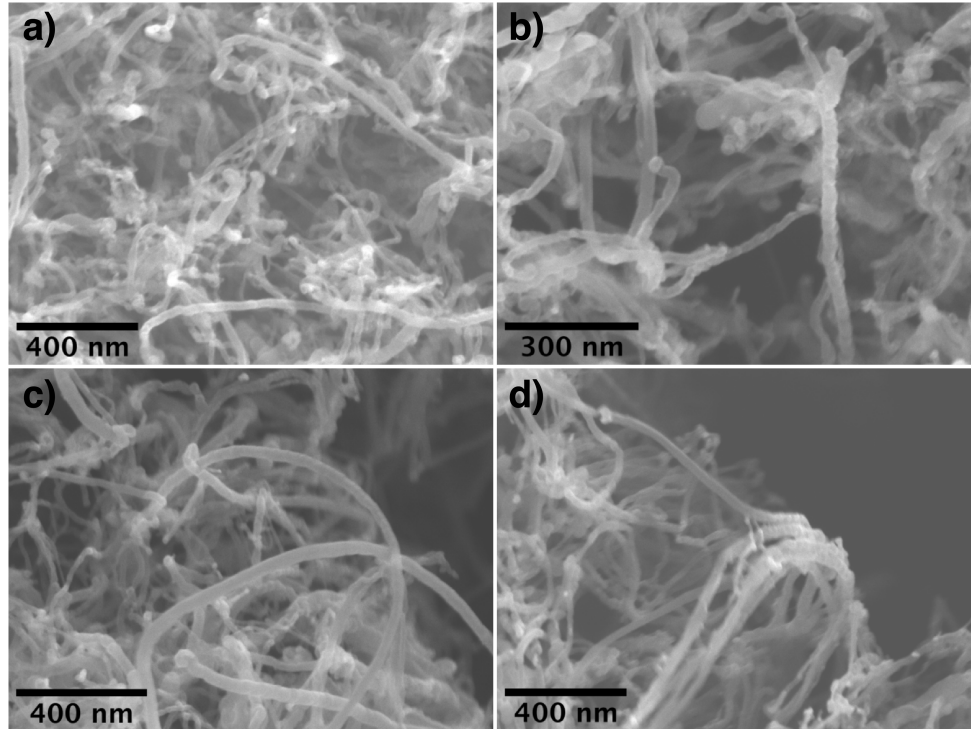


Figure 4.3: SEM of vertically-aligned carbon nanotubes irradiated with nitrogen ion at different acceleration voltages: a) 0.5 eV, b) 1.0 eV, c) 1.5 eV and d) 2.5 eV.

To study the influence of nitrogen ion irradiation at different acceleration voltages on the vertically-aligned CNTs, XPS analysis was performed. To determine the atomic percentage of nitrogen, oxygen and carbon in the samples, it was necessary to calculate the area of each peak per sample and estimate their contribution relative to the other regions as shown in Figure 4.4, for the analysis of these samples a Shirley background was used. The XPS surveys show that for an acceleration voltage of 0.5 eV the atomic concentrations are the following: 8.83 %O, 86.25 %C, and 4.92 %N. For an acceleration voltage of 1.0 eV the atomic concentrations are: 7.51 %O, 90.34 %C, and 2.16 %N. For an acceleration voltage of 1.5 eV the atomic concentrations are: 8.47 %O, 88.63 %C, and 2.90 %N. Lastly, for an acceleration voltage of 2.5 eV the atomic concentrations are: 11.26 %O, 81.38 %C, and 7.35 %N.

These results show a clear correlation between the increment in nitrogen and oxygen concentration, even though the ion irradiation was performed just with nitrogen. This contamination by oxygen may be related to the fact that not all the defects created by the nitrogen ions during the irradiation were exclusively containing a nitrogen atoms, the irradiation could have created some reactive sites that reacted with the oxygen coming from the environment.

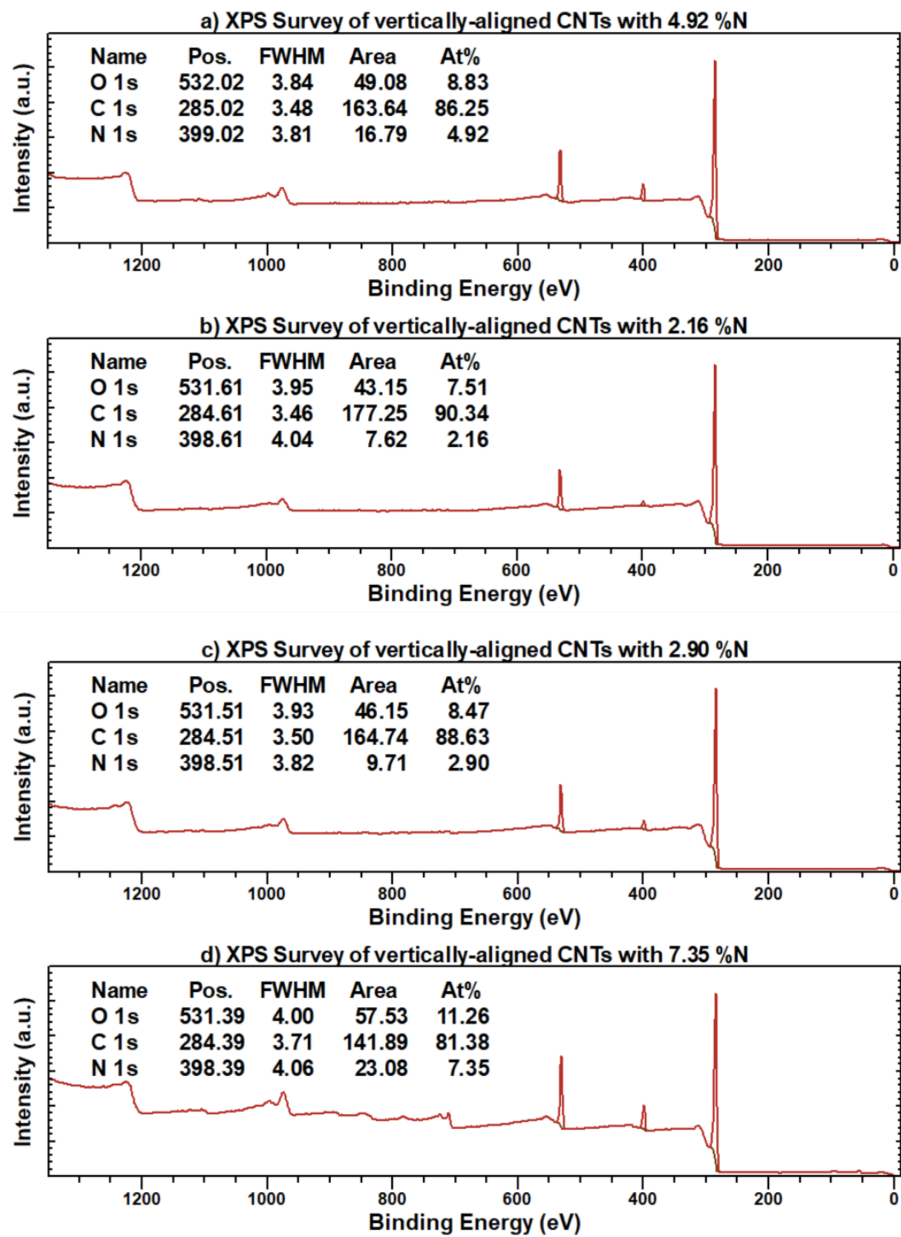


Figure 4.4: XPS survey of vertically-aligned CNTs with different nitrogen concentrations: a) 4.92%, b) 2.16%, c) 2.90% and d) 7.35%.

### 4.2.1 Nitrogen Concentration as a function of the acceleration voltage of the Nitrogen Ions

As shown in Figure 4.5, the experiments do not show a clear correlation between variation in the acceleration voltage and the nitrogen concentration in the vertically-aligned carbon nanotubes. One factor that was not taking into account but could have affected the results is the rest time after the ion irradiation. Further research should be done before concluding there is no relation between the acceleration voltage and the nitrogen content.

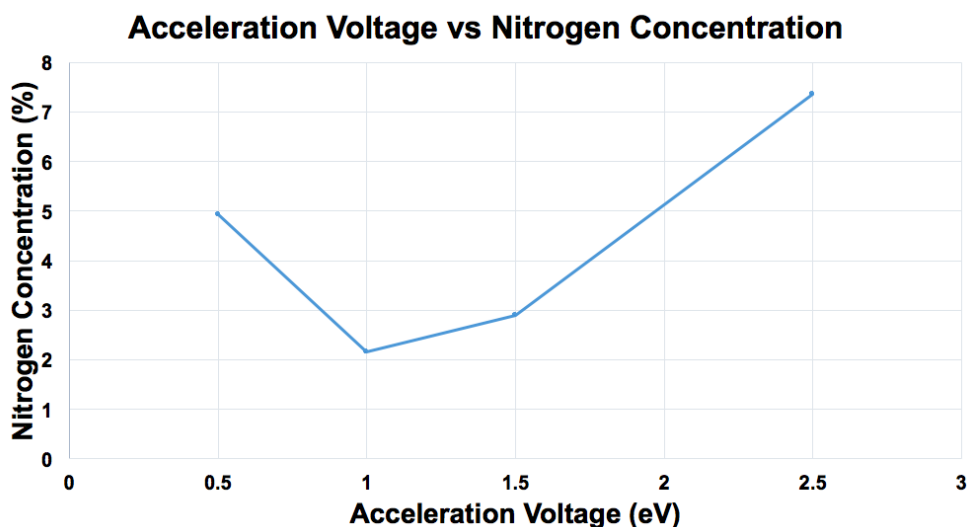


Figure 4.5: Nitrogen content as a function of the acceleration voltage.

### 4.2.2 N 1s & O 1s core level spectra analysis

For the analysis of the N 1s and O 1s core level spectra, all XPS experiments were calibrated respect to the main peak of the their respective C1s at 284.5 eV. This is not completely reliable, it is better to have an external standard calibrations, such as: gold. Since we are using a set calibration for the C 1s it will be not possible to measure the shift in the peaks as a function of the ion irradiation. To be able to make a better analysis, it would be advisable to do an external calibration with gold. Nevertheless, it is still possible to determine the chemical environment of the CNTs after the irradiation.

The N 1s spectra of the different experiments shown in Figure 4.6 present generally 5 components, N1 and N2 correspond to pyridinic and pyrrolic nitrogen defects respectively, N3 and N4 correspond to graphitic-center nitrogen and graphitic-valley nitrogen respectively, and N5 should correspond to a nitrogen-oxide groups.<sup>14,90,93-96</sup>

The results show an evolution of the pyrrolic defect as we increase the nitrogen concentration, at the same time the component corresponding to nitrogen-oxide groups follows an inverse proportion respect the increase of the nitrogen concentration until it disappears in the experiment with higher nitrogen concentration. The radius between the two main components N1 and N2 remain very stable as we change the nitrogen concentration. N4 seems to follow the

same inverse proportion as N5 respect to the increase of Nitrogen concentration, except for the last experiment where the nitrogen concentration is the highest among all the experiments where N5 increases showing a direct proportion.

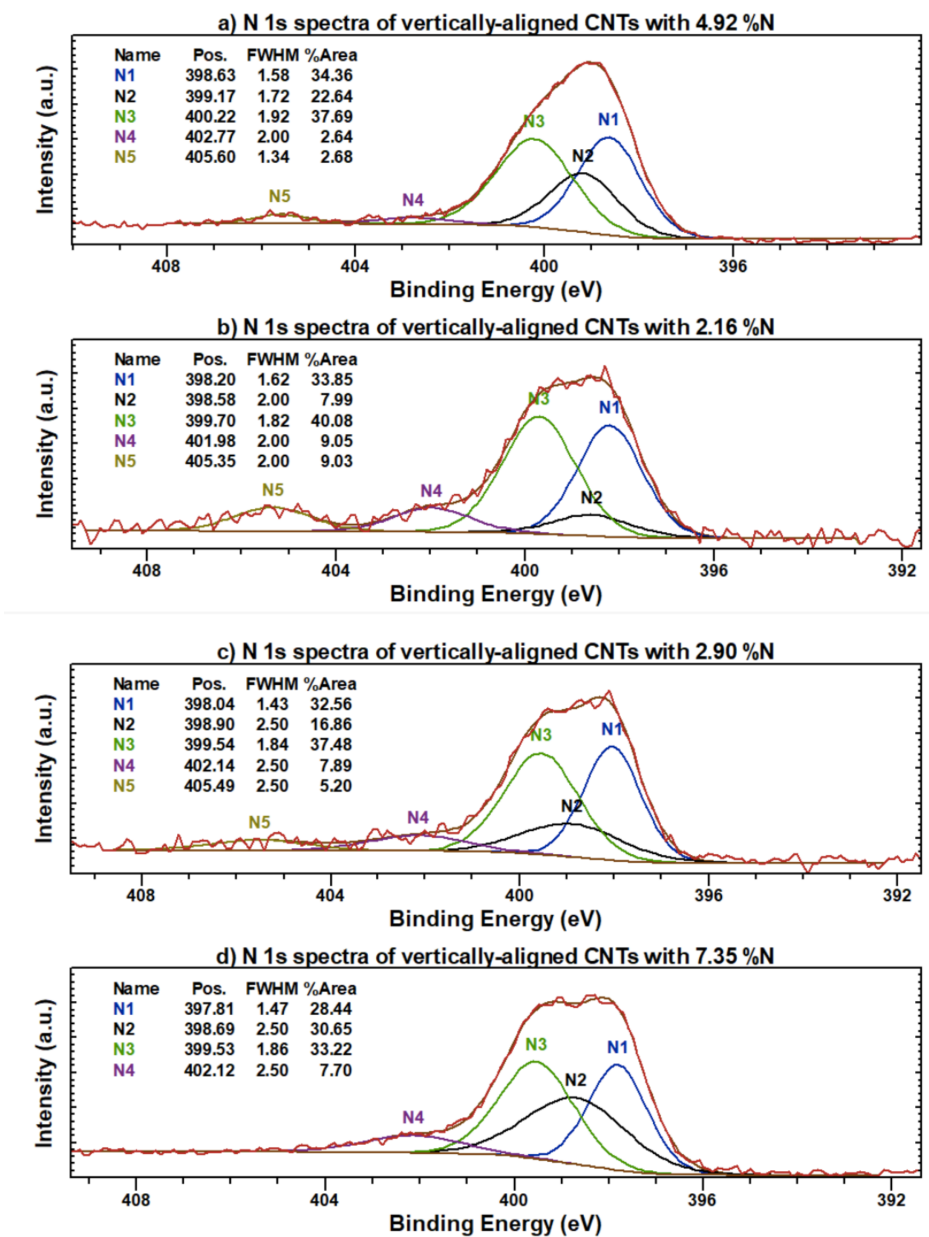


Figure 4.6: High resolution N1s deconvoluted core level spectra of vertically aligned carbon nanotubes irradiated with nitrogen ions at different acceleration voltages: a) 0.5 eV, b) 1.0 eV, c) 1.5 eV and d) 2.5 eV.

The O 1s spectra of the different experiments shown in Figure 4.7 present 4 components, O1 corresponds to C=N

bonding, O2 corresponds to C-OH bonding, O3 correspond to O=C-O and O4 corresponds to O-H groups. This graphs present a very stable evolution of all the components. Being the most prominent C-OH component and the O=C-O component.<sup>88,89,97-101</sup>

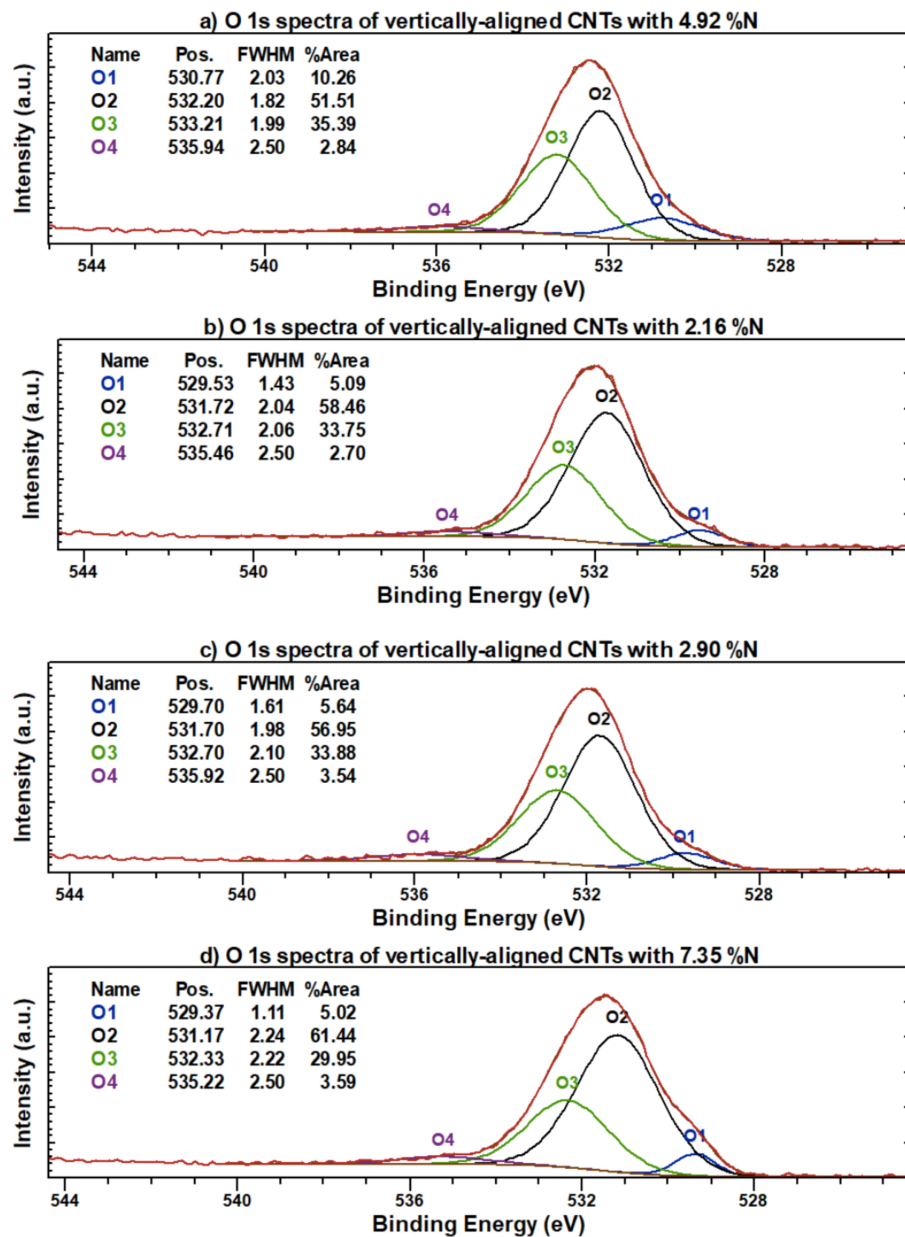


Figure 4.7: High resolution O1s deconvoluted core level spectra of vertically aligned carbon nanotubes irradiated with nitrogen ions at different acceleration voltages: a) 0.5 eV, b) 1.0 eV, c) 1.5 eV and d) 2.5 eV.

### 4.3 DFT calculations: XPS simulated spectra

In order to check the reliability of the sources used to deconvolute the N 1s, we perform XPS simulations using two different methods: Real space and Partial waves. We used two different methods to compare which method would fit better the experimental data. We chose a (8,4) SWCNT with different nitrogen defects as our system to simulate the core level spectra, as shown in Figure 4.8.

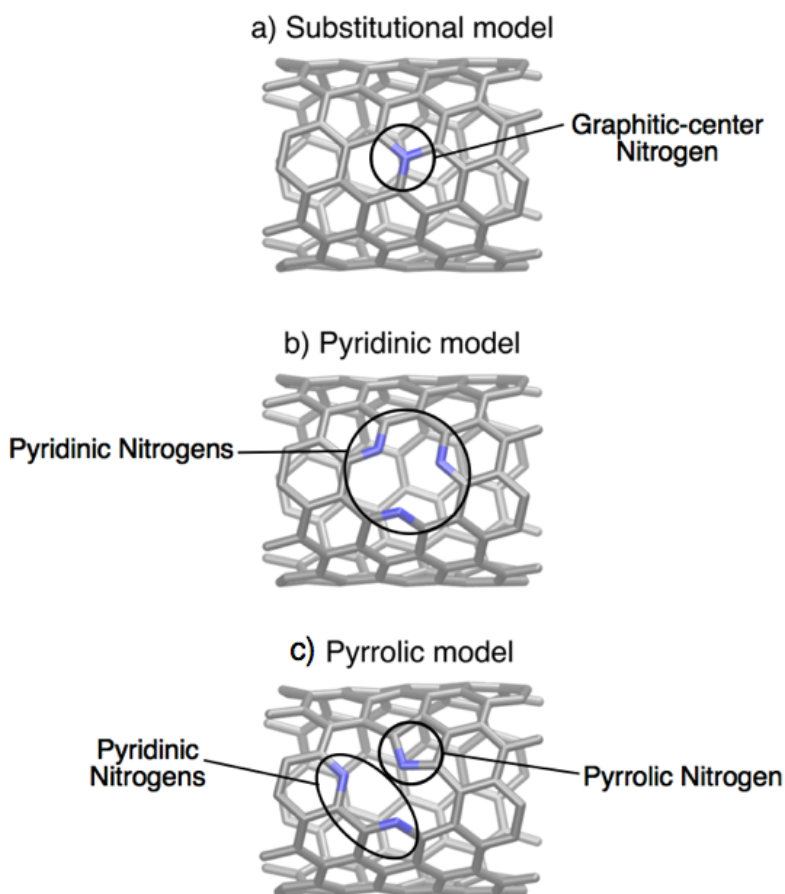


Figure 4.8: Schematics of SWCNTs (8,4) doped with different types of nitrogen defects: a) substitutional, b) pyridinic and c) pyrrolic.

All spectra were calibrated setting the C 1s peak at zero energy. The C 1s shown in Figure 4.9 (right side) shows the main peak corresponding to the C=C  $sp^2$ , while the little component at higher energy corresponds to the contribution of the nearest-neighbor to the nitrogen, the other little component present in all three models at a lower

energy than the nearest-neighbor corresponds to the next-nearest-neighbor to the nitrogen. Moreover, The C1s also shows that both method, even though they present the same form for the C 1s, there is a variation in energy respect to each other. The variation between these two methods is around 0.3 eV for the nearest-neighbor component.

The N 1s simulated spectra shows a consistency in the shape of the peaks. Nevertheless, taking the C 1s again as our reference energy, we notice that the difference in the N 1s energy for each method varies by around 1.2 eV.

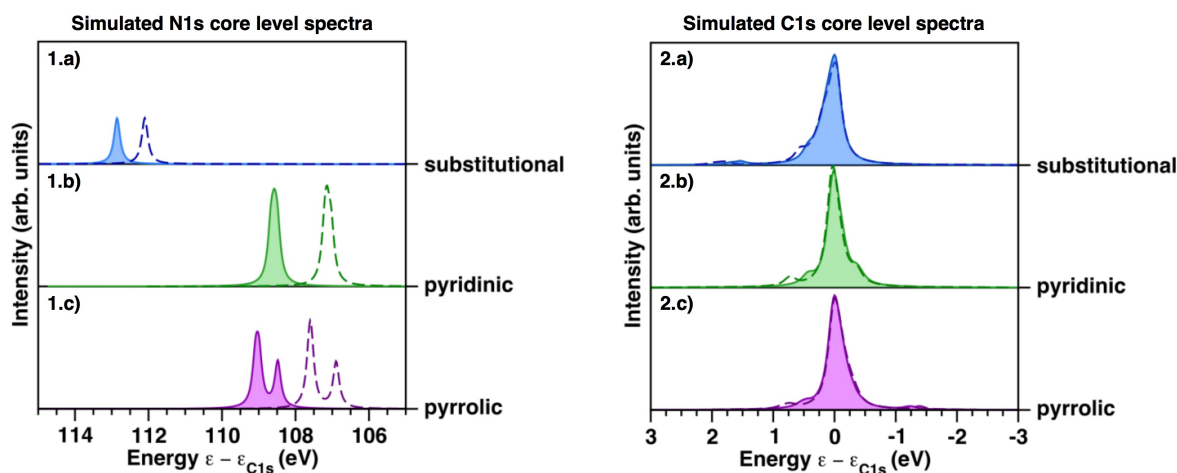


Figure 4.9: Simulated 1) N 1s and 2) C 1s XPS of a (8,4) SWCNT with a) substitutional, b) pyridinic and c) pyrrolic defects using real space method (straight line) and partial waves method (dotted line).

In Figure 4.10 we combine experimental XPS and simulated XPS. As expected Real Space calculations show the best fit for the experimental data. However, contrary to what it is stated in the literature, the pyrrolic nitrogen is at lower energy compared to the pyridine, suggesting that the energy stated in the literature of this two peaks are switched. Besides, our simulated graphitic-center matches better to what is stated in the literature as graphitic-valley. Further research should be done before concluding these new proposals.

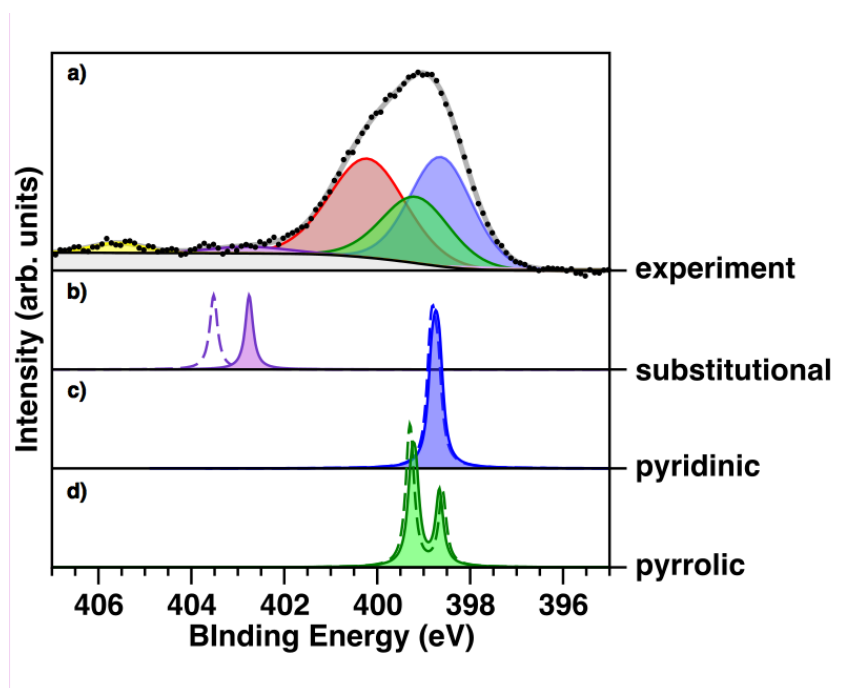


Figure 4.10: a) N 1s core level spectra of vertically-aligned CNTs irradiated with nitrogen at an acceleration voltage of 0.5 eV. Simulated N 1s core level spectra of a (8,4) SWCNT doped with different types nitrogen defects: b) substitutional, c) pyridinic and d) pyrrolic.



## Chapter 5

# Conclusions & Outlook

The SEM micrographs exhibit a bamboo-like structure in the carbon nanotubes corresponding to the different experiments performed, showing that the nitrogen atoms were introduced into the hexagonal lattice of the carbon nanotubes.

The XPS analysis clearly shows the influences of the ion irradiation on the vertically-aligned carbon nanotubes as well. Extra analysis could have been done if we would have performed an external calibration. Nevertheless, some interesting results appeared. Even though there is not a clear correlation between the acceleration voltage and nitrogen concentration. The relation between nitrogen content and oxygen content maintain a positive slope. Furthermore, we were able to obtain the chemical environment of the vertically-aligned carbon nanotubes, the deconvolution of the N 1s shows the presence of pyridinic, pyrrolic, graphitic-center, graphitic-valley, and nitrogen oxide groups; and how the pyrrolic component increase as a function of the nitrogen content, while the nitrogen oxide groups decrease as a function of the nitrogen content.

Above all, the XPS calculations show that the method that better fit the experimental data is Real Space, but Partial Waves show a decent approximation to Real Space calculations, showing that we can perform reliable calculations using a relative simple basis set, instead of using more descriptive basis set as DZP that do not work for core level calculations. Even more significantly the Real Space calculations propose a different explanation for the different components of the N 1s spectra.



## Appendix A

# Nitrogen-Doped Carbon Nanotubes Structures

### A.1 Substitutional model

Positions of the atoms of the substitutional model are shown in Table A.1

	x	y	z
0 C	13.343556	9.146772	-0.001461
1 C	13.108669	10.536546	11.062070
2 C	13.323348	9.614045	2.430128
3 C	12.932986	10.970433	2.158305
4 C	13.231239	10.073527	4.862367
5 C	12.661559	11.358427	4.586327
6 C	13.099366	10.530950	7.280265
7 C	12.400526	11.754957	7.007451
8 C	12.932855	10.973189	9.714657
9 C	12.122117	12.129008	9.441749
10 C	12.700123	11.383977	0.810303
11 C	11.762606	12.434570	0.542149
12 C	12.424545	11.756510	3.237234
13 C	11.384454	12.708029	2.980347
14 C	12.058032	12.068855	5.664774
15 N	10.950490	12.897984	5.391978
16 C	11.771070	12.442559	8.099313
17 C	10.539370	13.118133	7.808915

---

18 C	11.379570	12.709061	10.528424
19 C	10.081481	13.244156	10.247261
20 C	10.967724	12.940615	1.628679
21 C	9.619187	13.328739	1.346966
22 C	10.530799	13.090180	4.063681
23 C	9.152780	13.333528	3.784654
24 C	10.078433	13.207198	6.465662
25 C	8.682529	13.286586	6.200059
26 C	9.615728	13.324420	8.893980
27 C	8.212106	13.241308	8.632374
28 C	9.147448	13.349186	-0.004439
29 C	7.759887	13.112143	11.064163
30 C	8.683664	13.322776	2.432015
31 C	7.328946	12.930841	2.160986
32 C	8.210550	13.209240	4.857334
33 C	6.912632	12.690661	4.586970
34 C	7.762641	13.105066	7.286563
35 C	6.527064	12.428614	7.015129
36 C	7.322669	12.932165	9.716500
37 C	6.176343	12.116339	9.446129
38 C	6.914650	12.701596	0.811929
39 C	5.863236	11.765172	0.539599
40 C	6.528833	12.424645	3.236784
41 C	5.587669	11.380231	2.966872
42 C	6.173214	12.110186	5.671017
43 C	5.357063	10.966071	5.399210
44 C	5.860200	11.764231	8.097990
45 C	5.177572	10.533546	7.827429
46 C	5.589194	11.380466	10.527577
47 C	5.046395	10.081734	10.256042
48 C	5.357907	10.968144	1.619883
49 C	4.965378	9.616233	1.348124
50 C	5.177203	10.531445	4.049713
51 C	4.939063	9.146055	3.777742
52 C	5.043750	10.078483	6.479867
53 C	4.962710	8.673260	6.207196
54 C	4.966536	9.615492	8.909118
55 C	5.043678	8.209767	8.636779

---

56 C	4.940451	9.144889	0.000291
57 C	5.177831	7.757605	11.065822
58 C	4.966249	8.674307	2.428776
59 C	5.355525	7.321969	2.157980
60 C	5.043068	8.208790	4.859401
61 C	5.585331	6.909685	4.587415
62 C	5.173634	7.755216	7.288964
63 C	5.856593	6.524541	7.017304
64 C	5.356814	7.321067	9.717285
65 C	6.170965	6.173079	9.445714
66 C	5.585799	6.908753	0.810227
67 C	6.522398	5.858260	0.538159
68 C	5.857621	6.524638	3.239233
69 C	6.906205	5.586241	2.968100
70 C	6.172329	6.173561	5.669088
71 C	7.319084	5.357192	5.397711
72 C	6.522559	5.856928	8.098353
73 C	7.754067	5.174793	7.827351
74 C	6.907298	5.586017	10.526837
75 C	8.206160	5.045092	10.255908
76 C	7.318738	5.356380	1.620095
77 C	8.670680	4.964787	1.348248
78 C	7.753680	5.174460	4.049652
79 C	9.141514	4.937332	3.777429
80 C	8.207611	5.043551	6.479056
81 C	9.612636	4.963968	6.207059
82 C	8.672092	4.965114	8.908454
83 C	10.077593	5.042992	8.636316
84 C	9.141559	4.939010	0.000770
85 C	10.529166	5.177944	11.066217
86 C	9.613001	4.965574	2.429222
87 C	10.965069	5.356955	2.158498
88 C	10.077500	5.043551	4.858435
89 C	11.376949	5.585955	4.586855
90 C	10.531111	5.172743	7.288950
91 C	11.762201	5.857516	7.017556
92 C	10.965739	5.357402	9.717888
93 C	12.112450	6.173411	9.446531

94 C	11.377751	5.587315	0.809859
95 C	12.428374	6.524485	0.537196
96 C	11.762693	5.857479	3.239519
97 C	12.700821	6.908469	2.968278
98 C	12.112480	6.173345	5.669216
99 C	12.927689	7.319957	5.398152
100 C	12.428740	6.523919	8.098135
101 C	13.111538	7.755664	7.826793
102 C	12.701174	6.909813	10.526667
103 C	13.239698	8.212645	10.254441
104 C	12.929078	7.321652	1.620292
105 C	13.318097	8.674355	1.348464
106 C	13.111186	7.755396	4.049331
107 C	13.348833	9.142984	3.776061
108 C	13.245351	8.205064	6.479738
109 C	13.315473	9.610388	6.206866
110 C	13.318374	8.678368	8.905748
111 C	13.236441	10.083431	8.632136

Table A.1: Coordinates in Å of a SWCNT with a substitutional or graphitic nitrogen.

## A.2 Pyridinic model

Positions of the atoms of the pyridinic model are shown in Table A.2

	x	y	z
0 C	13.305103	9.158076	-0.004086
1 C	13.079649	10.549746	11.057351
2 C	13.278639	9.631781	2.433411
3 C	12.911369	11.004621	2.177278
4 C	13.185997	10.075556	4.863242
5 C	12.755916	11.432895	4.644813
6 C	13.065778	10.521117	7.277634
7 C	12.503746	11.805753	6.945307
8 C	12.902783	10.980967	9.701013
9 C	12.108029	12.146730	9.390498
10 C	12.692568	11.403357	0.808982

---

11 C	11.773616	12.459638	0.509812
12 C	12.457699	11.823788	3.265684
13 C	11.350258	12.720718	2.959662
14 N	12.428816	12.259772	5.671670
15 C	11.788915	12.487997	8.035403
16 C	10.501916	13.135163	7.789000
17 C	11.381655	12.726942	10.495655
18 C	10.077109	13.258172	10.244738
19 C	10.973205	12.949218	1.591342
20 C	9.616919	13.313582	1.330723
21 N	10.531083	13.050514	3.980486
22 C	9.223805	13.258384	3.751087
23 N	10.058934	13.287119	6.523473
24 C	8.741685	13.251676	6.250661
25 C	9.607203	13.315857	8.902400
26 C	8.207302	13.214387	8.639280
27 C	9.138133	13.354145	-0.014924
28 C	7.750223	13.110928	11.063373
29 C	8.689253	13.287103	2.415324
30 C	7.336735	12.909724	2.158167
31 C	8.290975	13.193015	4.870971
32 C	6.989507	12.661671	4.600120
33 C	7.771241	13.053111	7.296989
34 C	6.540855	12.390281	7.021358
35 C	7.309520	12.922193	9.719784
36 C	6.164037	12.108438	9.449422
37 C	6.907507	12.697300	0.811248
38 C	5.856349	11.763207	0.542518
39 C	6.564627	12.404339	3.250170
40 C	5.611383	11.372647	2.977491
41 C	6.210499	12.086806	5.671126
42 C	5.373149	10.959381	5.400488
43 C	5.851963	11.748929	8.101298
44 C	5.161566	10.526557	7.831156
45 C	5.573290	11.378039	10.532216
46 C	5.031888	10.079106	10.261571
47 C	5.362531	10.966912	1.628370
48 C	4.966219	9.616836	1.354987

---

49 C	5.188871	10.523496	4.053052
50 C	4.940719	9.142785	3.780864
51 C	5.037999	10.075837	6.481087
52 C	4.956510	8.671275	6.209816
53 C	4.948287	9.610705	8.914193
54 C	5.033131	8.206851	8.641597
55 C	4.933283	9.144019	0.006451
56 C	5.171713	7.757397	11.070933
57 C	4.965855	8.672245	2.432188
58 C	5.354722	7.321270	2.161323
59 C	5.040677	8.205289	4.862438
60 C	5.583560	6.908070	4.590693
61 C	5.168003	7.754481	7.292397
62 C	5.854850	6.527013	7.020837
63 C	5.351056	7.320317	9.721832
64 C	6.169755	6.176218	9.449873
65 C	5.584695	6.908974	0.813295
66 C	6.520898	5.859005	0.541395
67 C	5.856976	6.523889	3.241835
68 C	6.904224	5.585303	2.971079
69 C	6.171009	6.173825	5.672538
70 C	7.316902	5.357115	5.401606
71 C	6.522284	5.861338	8.101759
72 C	7.751879	5.176365	7.831175
73 C	6.906305	5.588109	10.529606
74 C	8.202538	5.042350	10.258998
75 C	7.315541	5.354083	1.622461
76 C	8.664969	4.956349	1.350613
77 C	7.750464	5.172051	4.052858
78 C	9.136150	4.924858	3.780383
79 C	8.204699	5.041713	6.482486
80 C	9.608604	4.951925	6.210344
81 C	8.668645	4.961575	8.911384
82 C	10.074202	5.030213	8.639439
83 C	9.136845	4.928508	0.003238
84 C	10.526148	5.161730	11.069326
85 C	9.606714	4.951232	2.431436
86 C	10.958350	5.342281	2.160298

87 C	10.072644	5.026912	4.860342
88 C	11.372600	5.565485	4.588104
89 C	10.527957	5.157205	7.291699
90 C	11.761369	5.837872	7.019726
91 C	10.962727	5.342494	9.721240
92 C	12.106136	6.162216	9.451143
93 C	11.370329	5.576890	0.812470
94 C	12.409819	6.526413	0.541691
95 C	11.754709	5.843540	3.240226
96 C	12.677848	6.908170	2.967270
97 C	12.107030	6.155102	5.669741
98 C	12.906031	7.312716	5.397455
99 C	12.422009	6.508484	8.100596
100 C	13.089138	7.746983	7.828029
101 C	12.682773	6.908801	10.531210
102 C	13.208091	8.216534	10.258563
103 C	12.897264	7.334383	1.621952
104 C	13.275537	8.692857	1.350569
105 C	13.069482	7.759201	4.047876
106 C	13.281057	9.149008	3.776734
107 C	13.215859	8.195362	6.479506
108 C	13.275101	9.603814	6.204396
109 C	13.279498	8.673811	8.907145
110 C	13.187257	10.074967	8.630020

Table A.2: Coordinates in Å of a SWCNT with a pyridinic nitrogen.

### A.3 Pyrrolic model

Positions of the atoms of the pyrrolic model are shown in Table A.3

	x	y	z
0 C	13.289939	9.161798	0.096256
1 C	13.083599	10.555664	11.186866
2 C	13.217252	9.640173	2.536801
3 C	12.823684	11.003779	2.305207
4 C	13.159689	10.086286	4.961183
5 C	12.722984	11.438398	4.753721

---

6 C	13.117278	10.545305	7.380701
7 C	12.610481	11.853398	7.060548
8 C	12.969012	10.987572	9.831338
9 C	12.224311	12.169541	9.554861
10 C	12.651313	11.407212	0.940615
11 C	11.757846	12.484328	0.668456
12 C	12.339527	11.820929	3.399998
13 C	11.255337	12.753757	3.148160
14 N	12.467452	12.286422	5.792286
15 C	11.900486	12.518492	8.190440
16 N	10.738612	13.115640	7.917244
17 C	11.458422	12.760989	10.620303
18 C	10.175342	13.279147	10.273300
19 C	10.918531	12.990773	1.738654
20 C	9.590160	13.389362	1.330219
21 C	10.261766	13.163091	4.149530
22 C	8.966209	13.503861	3.654341
23 N	10.142507	12.922254	5.515626
24 C	8.830513	13.090323	5.902022
25 C	9.811693	13.265241	8.891365
26 C	8.427350	13.074310	8.510960
27 C	9.186205	13.380670	-0.036974
28 C	7.822056	13.091799	10.960879
29 C	8.563296	13.445712	2.320272
30 C	7.226339	13.014486	2.036938
31 C	8.053981	13.334187	4.718891
32 C	6.793508	12.760861	4.479892
33 C	8.047385	12.875960	7.132718
34 C	6.728389	12.301714	6.904084
35 C	7.490052	12.826891	9.589737
36 C	6.330469	12.024867	9.338451
37 C	6.906479	12.718792	0.680449
38 C	5.883196	11.751860	0.428018
39 C	6.413678	12.505557	3.121068
40 C	5.534437	11.404122	2.872386
41 C	6.198953	12.077751	5.587884
42 C	5.364293	10.951874	5.327070
43 C	6.027419	11.677606	7.995324

---

44 C	5.249896	10.498904	7.745557
45 C	5.667235	11.342255	10.419272
46 C	5.081706	10.061571	10.173471
47 C	5.348253	10.975211	1.521798
48 C	4.967569	9.616697	1.275193
49 C	5.148058	10.544107	3.969442
50 C	4.928057	9.151197	3.715548
51 C	5.069797	10.053433	6.407314
52 C	4.957372	8.652852	6.149888
53 C	4.995964	9.594490	8.833178
54 C	5.037035	8.187172	8.581423
55 C	4.945486	9.139285	-0.068551
56 C	5.170436	7.748766	11.017623
57 C	4.959827	8.679693	2.368073
58 C	5.355782	7.325842	2.115986
59 C	5.034259	8.204145	4.800916
60 C	5.581025	6.906259	4.548595
61 C	5.161514	7.732336	7.236446
62 C	5.845336	6.502675	6.984115
63 C	5.344609	7.304516	9.673347
64 C	6.161476	6.156298	9.421095
65 C	5.583039	6.908553	0.772233
66 C	6.519171	5.855893	0.519714
67 C	5.856854	6.527387	3.203054
68 C	6.904185	5.586715	2.951960
69 C	6.164275	6.164191	5.636713
70 C	7.312902	5.348304	5.386364
71 C	6.511289	5.839000	8.075487
72 C	7.745321	5.158848	7.823777
73 C	6.900259	5.576963	10.510902
74 C	8.198279	5.031738	10.257935
75 C	7.313642	5.353401	1.607264
76 C	8.662731	4.949298	1.354028
77 C	7.746760	5.167891	4.041265
78 C	9.132918	4.917310	3.789325
79 C	8.197512	5.030193	6.477386
80 C	9.603118	4.942929	6.226390
81 C	8.662239	4.948146	8.912984

---

82 C	10.069960	5.025049	8.660729
83 C	9.132688	4.921819	0.009769
84 C	10.521760	5.161511	11.095143
85 C	9.602830	4.941450	2.443388
86 C	10.954626	5.334979	2.191926
87 C	10.066231	5.018960	4.879885
88 C	11.365891	5.561377	4.628276
89 C	10.521864	5.150450	7.316098
90 C	11.750852	5.841861	7.065075
91 C	10.956565	5.344311	9.750364
92 C	12.096751	6.171261	9.500329
93 C	11.364790	5.574413	0.847219
94 C	12.400982	6.531134	0.597394
95 C	11.745028	5.838162	3.283275
96 C	12.658655	6.911069	3.032221
97 C	12.093947	6.157442	5.718854
98 C	12.883281	7.322068	5.466540
99 C	12.405768	6.520533	8.153140
100 C	13.073439	7.761610	7.899856
101 C	12.671502	6.918851	10.590229
102 C	13.199868	8.227234	10.340902
103 C	12.876593	7.338280	1.690592
104 C	13.240282	8.700124	1.444911
105 C	13.040793	7.764095	4.121081
106 C	13.238701	9.156498	3.871538
107 C	13.196819	8.208255	6.554528
108 C	13.273602	9.618300	6.299648
109 C	13.278912	8.686267	8.988854
110 C	13.231894	10.089544	8.733908

Table A.3: Coordinates in Å of a SWCNT with a pyrrolic nitrogen.

# Bibliography

- [1] De Volder, M. F.; Tawfick, S. H.; Baughman, R. H.; Hart, A. J. Carbon nanotubes: present and future commercial applications. *science* **2013**, *339*, 535–539.
- [2] Futaba, D. N.; Hata, K.; Yamada, T.; Hiraoka, T.; Hayamizu, Y.; Kakudate, Y.; Tanaike, O.; Hatori, H.; Yumura, M.; Iijima, S. Shape-engineerable and highly densely packed single-walled carbon nanotubes and their application as super-capacitor electrodes. *Nature materials* **2006**, *5*, 987.
- [3] Chen, Z.; Higgins, D.; Chen, Z. Nitrogen doped carbon nanotubes and their impact on the oxygen reduction reaction in fuel cells. *Carbon* **2010**, *48*, 3057–3065.
- [4] Chen, H.; Roy, A.; Baek, J.-B.; Zhu, L.; Qu, J.; Dai, L. Controlled growth and modification of vertically-aligned carbon nanotubes for multifunctional applications. *Materials Science and Engineering: R: Reports* **2010**, *70*, 63–91.
- [5] Tong, T.; Zhao, Y.; Delzeit, L.; Kashani, A.; Meyyappan, M.; Majumdar, A. Dense vertically aligned multiwalled carbon nanotube arrays as thermal interface materials. *IEEE Transactions on Components and Packaging Technologies* **2007**, *30*, 92–100.
- [6] Jo, S.; Tu, Y.; Huang, Z.; Carnahan, D.; Wang, D.; Ren, Z. Effect of length and spacing of vertically aligned carbon nanotubes on field emission properties. *Applied Physics Letters* **2003**, *82*, 3520–3522.
- [7] Duesberg, G.; Graham, A.; Kreupl, F.; Liebau, M.; Seidel, R.; Unger, E.; Hoenlein, W. Ways towards the scaleable integration of carbon nanotubes into silicon based technology. *Diamond and related Materials* **2004**, *13*, 354–361.
- [8] Tasis, D.; Tagmatarchis, N.; Georgakilas, V.; Prato, M. Soluble carbon nanotubes. *Chemistry—A European Journal* **2003**, *9*, 4000–4008.
- [9] Singh, P.; Campidelli, S.; Giordani, S.; Bonifazi, D.; Bianco, A.; Prato, M. Organic functionalisation and characterisation of single-walled carbon nanotubes. *Chemical Society Reviews* **2009**, *38*, 2214–2230.
- [10] Ayala, P.; Arenal, R.; Rummeli, M.; Rubio, A.; Pichler, T. The doping of carbon nanotubes with nitrogen and their potential applications. *Carbon* **2010**, *48*, 575–586.

- [11] Jorio, A. In Carbon Nanotubes; Jorio, A., Dresselhaus, G., Dresselhaus, MS, Eds. *Topics in Applied Physics* **2008**,
- [12] Stephan, O.; Ajayan, P.; Colliex, C.; Redlich, P.; Lambert, J.; Bernier, P.; Lefin, P. Doping graphitic and carbon nanotube structures with boron and nitrogen. *Science* **1994**, *266*, 1683–1685.
- [13] Ewels, C.; Glerup, M. Nitrogen doping in carbon nanotubes. *Journal of nanoscience and nanotechnology* **2005**, *5*, 1345–1363.
- [14] Scardamaglia, M.; Amati, M.; Llorente, B.; Mudimela, P.; Colomer, J.-F.; Ghijsen, J.; Ewels, C.; Snyders, R.; Gregoratti, L.; Bittencourt, C. Nitrogen ion casting on vertically aligned carbon nanotubes: tip and sidewall chemical modification. *Carbon* **2014**, *77*, 319–328.
- [15] Cui, S.; Scharff, P.; Siegmund, C.; Schneider, D.; Risch, K.; Klötzer, S.; Spiess, L.; Romanus, H.; Schawohl, J. Investigation on preparation of multiwalled carbon nanotubes by DC arc discharge under N<sub>2</sub> atmosphere. *Carbon* **2004**, *42*, 931–939.
- [16] Van der Heide, P. *X-Ray photoelectron spectroscopy*; Wiley Online Library, 2011.
- [17] Lim, S.; Elim, H.; Gao, X.; Wee, A.; Ji, W.; Lee, J.; Lin, J. Electronic and optical properties of nitrogen-doped multiwalled carbon nanotubes. *Physical Review B* **2006**, *73*, 045402.
- [18] Mowbray, D. J.; Paz, A. P.; Ruiz-Soria, G.; Sauer, M.; Lacovig, P.; Dalmiglio, M.; Lizzit, S.; Yanagi, K.; Goldoni, A.; Pichler, T.; Ayala, P.; Rubio, A. Disentangling Vacancy Oxidation on Metallicity-Sorted Carbon Nanotubes. *The Journal of Physical Chemistry C* **2016**, *120*, 18316–18322.
- [19] Cabellos, J. L.; Mowbray, D. J.; Goiri, E.; El-Sayed, A.; Floreano, L.; De Oteyza, D.; Rogero, C.; Ortega, J. E.; Rubio, A. Understanding charge transfer in donor–acceptor/metal systems: A combined theoretical and experimental study. *The Journal of Physical Chemistry C* **2012**, *116*, 17991–18001.
- [20] Ruiz-Soria, G.; Perez Paz, A.; Sauer, M.; Mowbray, D. J.; Lacovig, P.; Dalmiglio, M.; Lizzit, S.; Yanagi, K.; Rubio, A.; Goldoni, A.; Ayala, P.; Pichler, T. Revealing the adsorption mechanisms of nitroxides on ultrapure, metallicity-sorted carbon nanotubes. *ACS nano* **2014**, *8*, 1375–1383.
- [21] Harris, P. J.; Harris, P. J. F. *Carbon nanotube science: synthesis, properties and applications*; Cambridge university press, 2009.
- [22] Jorio, A.; Dresselhaus, G.; Dresselhaus, M. S. *Carbon nanotubes: advanced topics in the synthesis, structure, properties and applications*; Springer Science & Business Media, 2007; Vol. 111.
- [23] Tanaka, K.; Iijima, S. *Carbon nanotubes and graphene*; Newnes, 2014.
- [24] Saito, R.; Dresselhaus, G.; Dresselhaus, M. *Physical properties of carbon nanotubes*; World scientific, 1998.

- [25] Lehman, J. H.; Terrones, M.; Mansfield, E.; Hurst, K. E.; Meunier, V. Evaluating the characteristics of multiwall carbon nanotubes. *Carbon* **2011**, *49*, 2581–2602.
- [26] Iijima, S. Helical microtubules of graphitic carbon. *Nature* **1991**, *354*, 56–58.
- [27] Nguyen, C. V.; Stevens, R. M.; Barber, J.; Han, J.; Meyyappan, M.; Sanchez, M. I.; Larson, C.; Hinsberg, W. D. Carbon nanotube scanning probe for profiling of deep-ultraviolet and 193 nm photoresist patterns. *Applied Physics Letters* **2002**, *81*, 901–903.
- [28] Smalley, R. E. *Carbon nanotubes: synthesis, structure, properties, and applications*; Springer Science & Business Media, 2003; Vol. 80.
- [29] Zhang, X.; Zhang, X.; Van Tendeloo, G.; Amelinckx, S.; De Beeck, M. O.; Van Landuyt, J. Carbon nanotubes; their formation process and observation by electron microscopy. *Journal of crystal growth* **1993**, *130*, 368–382.
- [30] Reznik, D.; Olk, C.; Neumann, D.; Copley, J. X-ray powder diffraction from carbon nanotubes and nanoparticles. *Physical review B* **1995**, *52*, 116.
- [31] Kharissova, O. V.; Kharisov, B. I. Variations of interlayer spacing in carbon nanotubes. *Rsc Advances* **2014**, *4*, 30807–30815.
- [32] Dresselhaus, M. S.; Dresselhaus, G.; Eklund, P. C. *Science of fullerenes and carbon nanotubes: their properties and applications*; Elsevier, 1996.
- [33] Fujita, M.; Saito, R.; Dresselhaus, G.; Dresselhaus, M. Formation of general fullerenes by their projection on a honeycomb lattice. *Phys. Rev. B* **1804**, *46*, 1992.
- [34] Serp, P.; Machado, B. *Nanostructured carbon materials for catalysis*; Royal Society of Chemistry, 2015.
- [35] Avouris, P.; Appenzeller, J.; Martel, R.; Wind, S. J. Carbon nanotube electronics. *Proceedings of the IEEE* **2003**, *91*, 1772–1784.
- [36] Li, J.; Stevens, R.; Delzeit, L.; Ng, H. T.; Cassell, A.; Han, J.; Meyyappan, M. Electronic properties of multiwalled carbon nanotubes in an embedded vertical array. *Applied Physics Letters* **2002**, *81*, 910–912.
- [37] Bandaru, P. R. Electrical properties and applications of carbon nanotube structures. *Journal of nanoscience and nanotechnology* **2007**, *7*, 1239–1267.
- [38] Datta, S. *Electronic transport in mesoscopic systems*; Cambridge university press, 1997.
- [39] Liu, K.; Avouris, P.; Martel, R.; Hsu, W. K. Electrical transport in doped multiwalled carbon nanotubes. *Phys. Rev. B* **2001**, *63*, 161404.
- [40] Ebbesen, T. W.; Ajayan, P. M. Large-scale synthesis of carbon nanotubes. *Nature* **1992**, *358*, 220–222.

- [41] Nikolaev, P.; Bronikowski, M. J.; Bradley, R. K.; Rohmund, F.; Colbert, D. T.; Smith, K.; Smalley, R. E. Gas-phase catalytic growth of single-walled carbon nanotubes from carbon monoxide. *Chemical physics letters* **1999**, *313*, 91–97.
- [42] Baker, T.; Murrell, L. *Novel materials in heterogeneous catalysis*; ACS Publications, 1990.
- [43] Kong, J.; Cassell, A. M.; Dai, H. Chemical vapor deposition of methane for single-walled carbon nanotubes. *Chemical Physics Letters* **1998**, *292*, 567–574.
- [44] Koley, G.; Cai, Z. Growth of Gallium Nitride Nanowires and Nanospirals. *MRS Online Proceedings Library Archive* **2006**, 963.
- [45] Chakrabarti, S.; Kume, H.; Pan, L.; Nagasaka, T.; Nakayama, Y. Number of walls controlled synthesis of millimeter-long vertically aligned brushlike carbon nanotubes. *The Journal of Physical Chemistry C* **2007**, *111*, 1929–1934.
- [46] Colomer, J.-F.; Ruelle, B.; Moreau, N.; Lucas, S.; Snyders, R.; Godfroid, T.; Navio, C.; Bittencourt, C. Vertically aligned carbon nanotubes: synthesis and atomic oxygen functionalization. *Surface and Coatings Technology* **2011**, *205*, S592–S596.
- [47] Kohn, W. Nobel lecture: Electronic structure of matter - wave functions and density functionals. *Rev. Mod. Phys.* **1999**, *71*, 1253–1266.
- [48] Perdew, J. P.; Ruzsinszky, A.; Tao, J.; Staroverov, V. N.; Scuseria, G. E.; Csonka, G. I. Prescription for the design and selection of density functional approximations: More constraint satisfaction with fewer fits. *The Journal of chemical physics* **2005**, *123*, 062201.
- [49] Kohn, W. Electronic structure of matter—wave functions and density functionals. *Rev. Mod. Phys.* **1999**, *71*, 1253–1266.
- [50] Pople, J. A. Nobel lecture: Quantum chemical models. *Reviews of Modern Physics* **1999**, *71*, 1267.
- [51] Gross, E.; Dreizler, R. Density functional theory: an approach to the quantum many-body problem. 1990.
- [52] Parr, R. G. *Horizons of Quantum Chemistry*; Springer, 1980; pp 5–15.
- [53] Koch, W.; Holthausen, M. C.; Holthausen, M. C. *A chemist's guide to density functional theory*; Wiley Online Library, 2001; Vol. 2.
- [54] Hohenberg, P.; Kohn, W. Inhomogeneous electron gas. *Physical review* **1964**, *136*, B864.
- [55] Kohn, W.; Sham, L. J. Self-Consistent Equations Including Exchange and Correlation Effects. *Phys. Rev.* **1965**, *140*, A1133–A1138.
- [56] Gunnarsson, O.; Lundqvist, B. I. Exchange and correlation in atoms, molecules, and solids by the spin-density-functional formalism. *Physical Review B* **1976**, *13*, 4274.

- [57] Ziegler, T.; Rauk, A.; Baerends, E. J. On the calculation of multiplet energies by the Hartree-Fock-Slater method. *Theoretica chimica acta* **1977**, *43*, 261–271.
- [58] Burke, K.; Perdew, J. P.; Ernzerhof, M. Why semilocal functionals work: Accuracy of the on-top pair density and importance of system averaging. *The Journal of chemical physics* **1998**, *109*, 3760–3771.
- [59] Capelle, K. A bird's-eye view of density-functional theory. *Brazilian Journal of Physics* **2006**, *36*, 1318–1343.
- [60] Perdew, J. P.; Burke, K.; Ernzerhof, M. Generalized gradient approximation made simple. *Physical review letters* **1996**, *77*, 3865.
- [61] Becke, A. D. Density-functional exchange-energy approximation with correct asymptotic behavior. *Physical review A* **1988**, *38*, 3098.
- [62] Csonka, G. I.; Perdew, J. P.; Ruzsinszky, A.; Philipsen, P. H.; Lebègue, S.; Paier, J.; Vydrov, O. A.; Ángyán, J. G. Assessing the performance of recent density functionals for bulk solids. *Physical Review B* **2009**, *79*, 155107.
- [63] Staroverov, V. N.; Scuseria, G. E.; Tao, J.; Perdew, J. P. Comparative assessment of a new nonempirical density functional: Molecules and hydrogen-bonded complexes. *The Journal of chemical physics* **2003**, *119*, 12129–12137.
- [64] Zhao, Y.; Truhlar, D. G. Design of density functionals that are broadly accurate for thermochemistry, thermochemical kinetics, and nonbonded interactions. *The Journal of Physical Chemistry A* **2005**, *109*, 5656–5667.
- [65] Marsman, M.; Paier, J.; Stroppa, A.; Kresse, G. Hybrid functionals applied to extended systems. *Journal of Physics: Condensed Matter* **2008**, *20*, 064201.
- [66] Heyd, J.; Peralta, J. E.; Scuseria, G. E.; Martin, R. L. Energy band gaps and lattice parameters evaluated with the Heyd-Scuseria-Ernzerhof screened hybrid functional. *The Journal of chemical physics* **2005**, *123*, 174101.
- [67] Brothers, E. N.; Izmaylov, A. F.; Normand, J. O.; Barone, V.; Scuseria, G. E. Accurate solid-state band gaps via screened hybrid electronic structure calculations. 2008.
- [68] Justscience, WHAT IS ION IMPLANTATION? 2017; <http://www.justscience.in/articles/what-is-ion-implantation/2017/07/31>.
- [69] JEOL-Ltd., JSM-7500/JSM-7500FA.
- [70] Krzyzanek, V.; Tacke, S.; Sporenberg, N.; Schönhoff, M.; Reichelt, R. Mass measurements using electron scattering employing an “in-lens” scanning electron microscope.
- [71] Knop-Gericke, A. X-ray Photoelectron Spectroscopy. An Introduction to Principles and Practices. By Paul van der Heide. *Angewandte Chemie International Edition* **2012**, *51*, 9218–9218.
- [72] Brundle, C. R.; Evans, C. A.; Wilson, S. *Encyclopedia of materials characterization: surfaces, interfaces, thin films*; Gulf Professional Publishing, 1992.

- [73] Gurker, N.; Ebel, M. F.; Ebel, H. Imaging XPS—A new technique, I—principles. *Surface and Interface Analysis* **1983**, *5*, 13–19.
- [74] XPS / ESCA. <https://www.phl.com/surface-analysis-techniques/xps-esca.html>.
- [75] Ward, R.; Wood, B. A comparison of experimental and theoretically derived sensitivity factors for XPS. *Surface and interface Analysis* **1992**, *18*, 679–684.
- [76] Physical-Electronics, VersaProbe III.
- [77] PHI VersaProbe III Scanning XPS Microprobe. <https://www.phl.com/surface-analysis-equipment/versaprobe.html>.
- [78] Végh, J. The Shirley-equivalent electron inelastic scattering cross-section function. *Surface science* **2004**, *563*, 183–190.
- [79] Peak Fitting in XPS. [http://www.casaxps.com/help\\_manual/manual\\_updates/peak\\_fitting\\_in\\_xps.pdf](http://www.casaxps.com/help_manual/manual_updates/peak_fitting_in_xps.pdf).
- [80] Ejaz, A.; Jeon, S. The individual role of pyrrolic, pyridinic and graphitic nitrogen in the growth kinetics of Pd NPs on N-rGO followed by a comprehensive study on ORR. *International Journal of Hydrogen Energy* **2018**, *43*, 5690–5702.
- [81] Strange, M.; Kristensen, I. S.; Thygesen, K. S.; Jacobsen, K. W. Benchmark Density Functional Theory Calculations for Nanoscale Conductance. *J. Chem. Phys.* **2008**, *128*, 114714.
- [82] Carbon. <https://wiki.fysik.dtu.dk/gpaw/setups/C.html>.
- [83] Nitrogen. <https://wiki.fysik.dtu.dk/gpaw/setups/N.html>.
- [84] Manual. <https://wiki.fysik.dtu.dk/gpaw/documentation/manual.html>.
- [85] Blöchl, P. E. Projector augmented-wave method. *Phys. Rev. B* **1994**, *50*, 17953–17979.
- [86] Cortez, S.; Sierra, A.; Bittencourt, C.; Colomer, J.-F.; Chacón-Torres, J.; Mowbray, D. Low-Kinetic Energy Ion Irradiation of vertically-aligned Carbon Nanotubes. **2019**, *In preparation*.
- [87] <https://srdata.nist.gov/xps/XPSDetailPage.aspx?AllDataNo=2729>.
- [88] Datsyuk, V.; Kalyva, M.; Papagelis, K.; Parthenios, J.; Tasis, D.; Siokou, A.; Kallitsis, I.; Galiotis, C. Chemical oxidation of multiwalled carbon nanotubes. *Carbon* **2008**, *46*, 833–840.
- [89] Tóth, A.; Voitko, K. V.; Bakalinska, O.; Prykhod'ko, G. P.; Bertóti, I.; Martínez-Alonso, A.; Tascón, J. M.; Gun'ko, V. M.; László, K. Morphology and adsorption properties of chemically modified MWCNT probed by nitrogen, n-propane and water vapor. *Carbon* **2012**, *50*, 577–585.

- [90] Maldonado, S.; Morin, S.; Stevenson, K. J. Structure, composition, and chemical reactivity of carbon nanotubes by selective nitrogen doping. *Carbon* **2006**, *44*, 1429–1437.
- [91] Li, Y.; Wang, J.; Li, X.; Liu, J.; Geng, D.; Yang, J.; Li, R.; Sun, X. Nitrogen-doped carbon nanotubes as cathode for lithium–air batteries. *Electrochemistry Communications* **2011**, *13*, 668–672.
- [92] Glerup, M.; Castignolles, M.; Holzinger, M.; Hug, G.; Loiseau, A.; Bernier, P. Synthesis of highly nitrogen-doped multi-walled carbon nanotubes. *Chemical Communications* **2003**, 2542–2543.
- [93] Deng, D.; Pan, X.; Yu, L.; Cui, Y.; Jiang, Y.; Qi, J.; Li, W.-X.; Fu, Q.; Ma, X.; Xue, Q. Toward N-doped graphene via solvothermal synthesis. *Chemistry of Materials* **2011**, *23*, 1188–1193.
- [94] Sharifi, T.; Hu, G.; Jia, X.; Wagberg, T. Formation of active sites for oxygen reduction reactions by transformation of nitrogen functionalities in nitrogen-doped carbon nanotubes. *ACS nano* **2012**, *6*, 8904–8912.
- [95] Tüci, G.; Zafferoni, C.; Rossin, A.; Luconi, L.; Milella, A.; Ceppatelli, M.; Innocenti, M.; Liu, Y.; Pham-Huu, C.; Giambastiani, G. Chemical functionalization of N-doped carbon nanotubes: a powerful approach to cast light on the electrochemical role of specific N-functionalities in the oxygen reduction reaction. *Catalysis Science & Technology* **2016**, *6*, 6226–6236.
- [96] Li, O. L.; Chiba, S.; Wada, Y.; Lee, H.; Ishizaki, T. Selective nitrogen bonding states in nitrogen-doped carbon via a solution plasma process for advanced oxygen reduction reaction. *RSC Advances* **2016**, *6*, 109354–109360.
- [97] Sobolkina, A.; Mechtcherine, V.; Bellmann, C.; Khavrus, V.; Oswald, S.; Hampel, S.; Leonhardt, A. Surface properties of CNTs and their interaction with silica. *Journal of colloid and interface science* **2014**, *413*, 43–53.
- [98] Zaman, S.; Hussain, S.; Butt, F. K.; Jianguo, X.; Zhu, C. Functionalization of Carbon Nanotubes by a Facile Chemical Method and Its Application in Anti-Diabetic Activity. *Journal of Nanoscience and Nanotechnology* **2017**, *17*, 8557–8561.
- [99] Ozturk, B.; de Luna-Bugallo, A.; Panaitescu, E.; Chiaramonti, A. N.; Liu, F.; Vargas, A.; Jiang, X.; Kharche, N.; Yavuzcetin, O.; Alnaji, M. Atomically thin layers of B–N–C–O with tunable composition. *Science Advances* **2015**, *1*, e1500094.
- [100] Kundu, S.; Wang, Y.; Xia, W.; Muhler, M. Thermal stability and reducibility of oxygen-containing functional groups on multiwalled carbon nanotube surfaces: a quantitative high-resolution XPS and TPD/TPR study. *The Journal of Physical Chemistry C* **2008**, *112*, 16869–16878.
- [101] Okpalugo, T.; Papakonstantinou, P.; Murphy, H.; McLaughlin, J.; Brown, N. High resolution XPS characterization of chemical functionalised MWCNTs and SWCNTs. *Carbon* **2005**, *43*, 153–161.